Journal of Groundwater Science and Engineering 12(2024) 360–386

Journal homepage: http://gwse.iheg.org.cn

Research Article

Morphometric analysis and hydrological implications of the Himalayan River Basin, Goriganga, India, using Remote Sensing and GIS techniques

Parvaiz Ahmad Ganie[1*], Ravindra Posti[1], Garima [1], Kishor Kunal[1], Nityanand Pandey[1], Pramod Kumar Pandey[1]

[1] *ICAR - Directorate of Coldwater Fisheries Research*, *Bhimtal*, *Nainital*, *Uttarakhand*- 263136, *India*.

Abstract: The application of Geographic Information System (GIS) methodologies offers valuable insights into the hydrological behaviour of watersheds through the analysis of their morphometric attributes. This study focuses on the Goriganga River, a major tributary of the Ganga River system, by conducting a detailed morphometric analysis using Advanced Spaceborne Thermal Emission and Reflection Radiometer (ASTER) imagery with 30 m resolution, alongside survey of India topographic sheets. Thirty-two watersheds within the river basin were delineated to calculate linear, areal, and relief morphometric parameters, covering a total drainage area of 2,183.11 km^2. The drainage pattern, primarily dendritic to sub-dendritic, is shaped by the region's topography, geological structure, and precipitation patterns. Classified as a 6th-order basin, the drainage density ranges from 1.21 km/km^2 to 1.96 km/km^2, underlining the significant influence of the regional physiography and lithological composition on the stream ordering. Relief analysis suggests the basin is in an early developmental stage, characterised by varying slope gradients and a low to moderate risk of soil erosion. The basin's hydrogeology is complex, with aquifer distribution primarily governed by lithological factors. Limestone, due to its high permeability and karst features, forms the principal aquifer, although it is susceptible to contamination. In contrast, groundwater potential in the Basement Gneissic Complex and Schist regions is limited to structurally controlled zones, while shale acts as an aquitard. The basin's heterogeneous aquifer characteristics emphasize the need for localized groundwater management strategies tailored to specific lithological units. The integration of remote sensing and GIS techniques effectively delineates the basin's morphometric and hydrogeological characteristics, providing critical information for the development of sustainable water resource management strategies.

Keywords: Advanced Spaceborne Thermal Emission and Reflection Radiometer; Survey of India; Toposheets; Linear; Areal; Relief; Drianage; Stream order; Hydrogeology

Received: 10 Dec 2023/ Accepted: 21 Sep 2024/ Published: 06 Dec 2024

Introduction

Water resources are essential to global sustainability, forming the foundation for development across various sectors. The growing demands of an increasing population, expanded irrigation systems, and rapid industrialization have notably intensified water usage, emphasizing the need for efficient water resource management (Shekar and Mathew, 2022). River basins, characterized by their river networks, are crucial geographical and functional units, representing the three-dimensional landscape and the dynamic processes that have shape them over millennia (Rai et al. 2017). These basins are vital for sustainable development, driven by an understanding of their morphometric attributes (Horton, 1945), and they also serve as biodiversity hotspots, harbouring rich reserves of soil, water, and biodiversity. The interaction between human activities and river basins highlights the importance of integrating basin manage-

*Corresponding author: Parvaiz Ahmad Ganie, *E-mail address*: parvaizahmad12@gmail.com

DOI: 10.26599/JGSE.2024.9280028

Ganie PA, Posti R, Garima, et al. 2024. Morphometric analysis and hydrological implications of the Himalayan River Basin, Goriganga, India, using Remote Sensing and GIS techniques. Journal of Groundwater Science and Engineering, 12(4): 360-386.

ment into sustainable resource utilization strategies (Krishnan and Ramasamy, 2022). Moreover, effective river basin management is crucial for ensuring food security, further highlighting the role of morphometric analysis in understanding hydrological and geological characteristics needed for improved watershed management (Ganie et al. 2023b).

Morphometry, the quantitative study of landforms, offers valuable insights into a basin's hydrological behavior and geological structure (Saha et al. 2022; Ganie et al. 2023). By analyzing the morphology of drainage systems, researchers can gather essential information to address hydrological challenges and promote sustainable water use (Abijith et al. 2020). This approach is particularly beneficial in regions where comprehensive hydrological and meteorological data are scarce, providing a reliable method for predicting hydrological hazards such as flash floods (Zhai et al. 2021). The geomorphological characteristics of river catchments, including size, structure, gradient, and river density, play a crucial role in shaping hydrological events, supporting soil and water conservation efforts, and facilitating natural resource management (Shekar and Mathew, 2022; Ganie et al. 2023a).

However, human interventions, such as unplanned construction, disrupt the natural hydrological cycles of river basins, leading to adverse physiographical effects. Although the geographical diversity in a drainage basin's morphology is primarily influenced by geological factors, human activities pose significant threats to water availability, quality, and river ecosystems (Kumar et al. 2018; Ganie et al. 2024a). The alteration of natural landscapes by anthropogenic activities highlights the need for a thorough examination of basin morphometry to develop strategies for sustainable land and water resource management (Guth, 2011; Rai et al. 2017; Ganie et al. 2024).

Historically, morphometric analysis relied on manual evaluations of topographic maps, a time-intensive process that, despite its limitations, provided valuable insights into river basin characteristics (Horton, 1932, 1945; Strahler, 1952, 1964; Schumm, 1956). The advent of geospatial and computational technologies has transformed this field, enabling more accurate and efficient assessments through the use of Digital Elevation Models (DEMs) and Geographic Information Systems (GIS) (Loritz et al. 2019; Ganie et al. 2023c). These technological advancements have made it possible to perform comprehensive analyses of hydrographs and morphology, significantly enhancing our understanding of interactions between drainage systems, geology, and landforms (Ganie et al. 2016; Tassew et al. 2021; Khatoon and Javed, 2022; Ganie et al. 2022).

In the Himalayan context, perennial rivers are crucial to North India, supplying essential water for drinking and agriculture, thus reducing the reliance on water imports. The Kali River, marking the border between India and Nepal, particularly benefits from the tributary waters of the Goriganga River. However, a detailed morphological analysis of the watersheds within the Goriganga Basin has been largely overlooked, highlighting the need to address watershed management issues. This study aims to analyze hydromorphological parameters to fill this knowledge gap, thereby establishing a foundation for informed decision-making in resource allocation for watershed management and conservation.

This research aims to conduct a comprehensive morphometric analysis of the Goriganga Basin using GIS techniques applied to remote sensing data, with the goal of enhancing the understanding of the hydro-geomorphic characteristics of this mountainous river basin. Despite the challenges of recording critical variables in the study area's remote location, this research highlights the importance of employing alternative methods while adhering to scientific principles. By utilizing digital elevation models, the study examines key hydromorphological parameters to inform watershed management planning without relying on complex models. This approach is crucial for effective water supply, demand, and flood management. By identifying essential hydro-morphometric parameters, this research seeks to improve water resource management and address issues related to water supply, demand, and flood control. The insights gained from this analysis are expected to facilitate optimal resource allocation in data-scarce mountainous river basins, paving the way for sustainable resource management strategies.

1 Study area

The research area is situated in the Eastern Kumaon district of Uttarakhand, India, demarcated by coordinates 79° 55' 00" N to 80° 30' 00" N and 29° 45' 6.3" E to 30° 35' 00" E (Fig. 1). The hydrology of the region is significantly influenced by two glaciers: The first, positioned near *Milam* at an elevation of 3,600 m above sea level, to the northeast of Nanda Devi, feeds the eastern branch of the river, while the second glacier, located near the *Untadhura* ridge, sustains the western branch

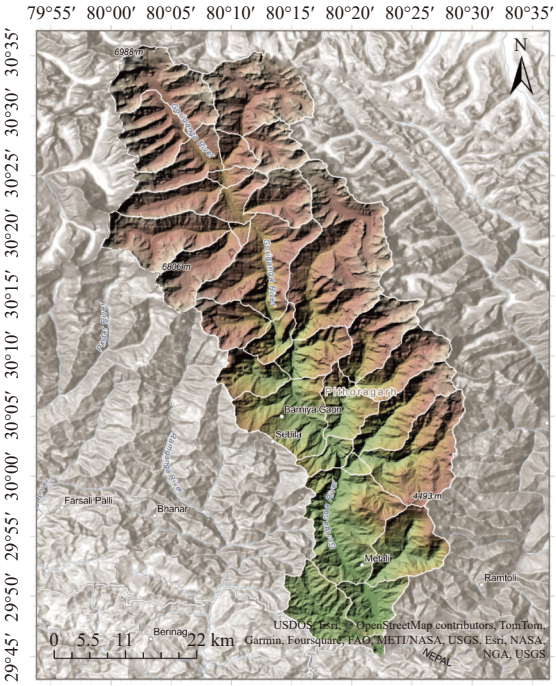

Fig. 1 Location map of the study area
(a) highlighting the state of Uttarakhand. (b) Map of Uttarakhand indicating the location of the Goriganga Basin. (c) Detailed map illustrating the Goriganga Basin

(Ashok, 2014). The region is bordered by the *Dhauliganga* River to the northeast and the Ramganga River to the southwest. The river predominantly flows southeastward until it merges with the Kali River at *Jauljibi,* with its northern reaches being glaciated. The river's trajectory generally follows a north-south direction, aligning with the transverse faults characteristic of the eastern Kumaon Himalayas (Ashok, 2014).

1.1 Geology

The geology of the Goriganga Basin is characterized by rocks oriented in a west-northwest to east-southeast direction. The area predominantly features a variety of metamorphic and sedimentary rocks, such as phyllites, schists, micaceous quartzites, amphibolites, and granitic gneisses (Valdiya, 1980). The principal rock formations in the basin include Tethyan sediments, gneisses and granitic rocks from the Vaikrita and Munsiari Formations, quartzites from the Berinag Formation, as well as Thalkedar limestone and Gangolihat dolomite (Joshi and kotlia, 2015). These formations are interspersed with major geological faults, including the Main Central Thrust, Vaikrita Thrust, Munsiari Thrust, Berinag Thrust, Chhiplakot Thrust, and the North Almora Thrust (Valdiya, 1976) (Fig. 2).

A notable features of the Goriganga Basin is the network of streams and gorges oriented in a north-northwest to south-southeast direction. These are characterized by straight mountain fronts, fault scarps, and steep cliffs, particularly in the middle and lower sections of the basin. Other significant landforms include rock benches, waterfalls, and deeply cut meanders, with smaller streams generally following a north-northeast to south-southwest direction. This orientation suggests that the landform development in the area is strongly influenced by the underlying geological structure. Additionally, river terraces formed by sediment deposition are present along both banks of the river.

1.2 Hydrogeology

The basin is characterized by four main rock types: The Basement Gneissic Complex, Limestone, Schist, and Shale. The Basement Gneissic Complex and Schist, with low porosity and permeability, store and transmit groundwater primarily through fractures and weathered zones. In contrast, limestone, due to its susceptibility to karstification, forms highly permeable aquifers with significant potential for groundwater storage and flow. Shale, acting as an impermeable aquitard, restricts groundwater movement and serves to protect underlying aquifers from contamination.

1.3 Climate

The climatic conditions in the area exhibit substantial variability, ranging from tropical warm temperate climates to the cold alpine conditions, including glaciated and perpetually frozen zones at different altitudes. The geographical composition of the region includes 50% under permanently frozen and glaciated conditions, 20% within the alpine zone, and 18% in the cold temperate and cold zones. Temperature variations range from 0 to 30°C throughout the year, with peaks occurring in June and the lowest temperatures in January. Precipitation data from 2020 indicate an average annual rainfall of 659.96 mm, with a maximum of 965.55 mm, primarily occurring during the southwest monsoon in May (Das, 2015).

The river basin plays a pivotal role in meeting the drinking water and industrial needs of Pithoragarh and fulfilling the irrigation demands of surrounding villages. Furthermore, the river's diverse fish populations support the local econ-

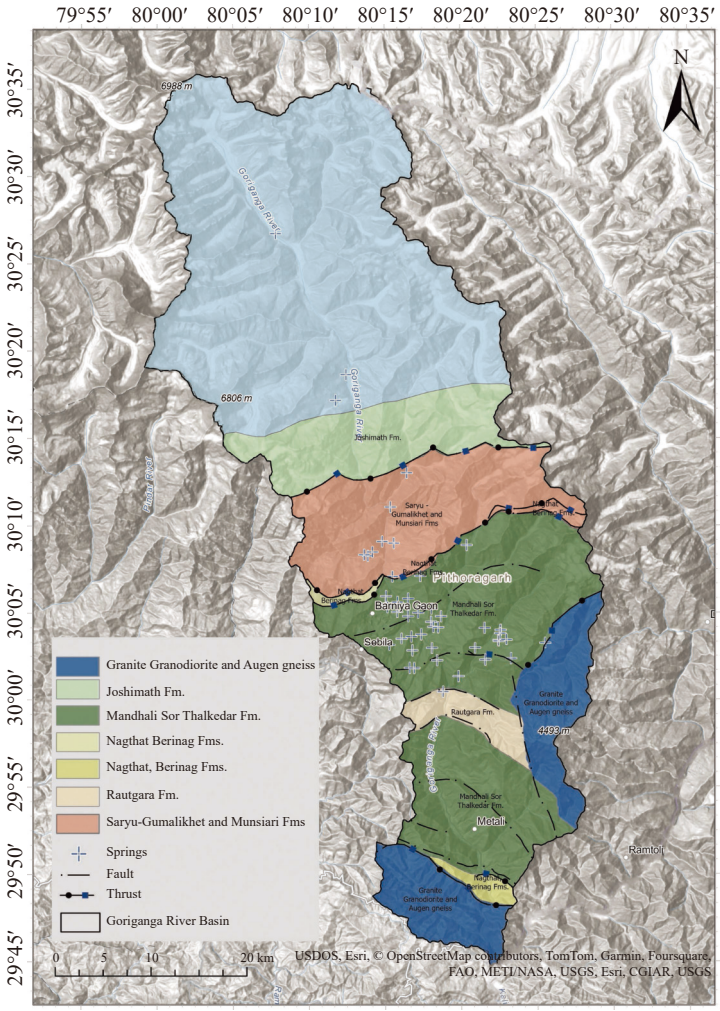

Fig. 2 Geology of the Goriganga Basin

omy through fishing, aqua-tourism, and fisheries-related enterprises. However, escalating water demands, especially for drinking and irrigation purposes, have led to the over-exploitation of groundwater resources within the basin. The primary mechanisms replenishing the basin's aquifers include return flows from agricultural irrigation, direct precipitation, and river bed infiltration, among other sources.

2 Data

The study employed a quantitative morphometric analysis of the Goriganga drainage basin using satellite data from the Advanced Spaceborne Thermal Emission and Reflection Radiometer (ASTER) Digital Elevation Model (DEM). ASTER was launched on NASA's Terra spacecraft in December 1999 and captures data across three spectral bands: Visible Near-Infrared (VNIR), ShortWave Infrared (SWIR), and Thermal Infrared (TIR), with ground resolutions of 15 m, 30 m, and 90 m, respectively.

The original ASTER data were enhanced by incorporating 260,000 overlapping images, which improved spatial resolution, reduced data errors, and provide more accurate coverage of water bodies (ASTER, 2011). ASTER offers global coverage from 83 degrees north to 83 degrees south (Abrams and Hook, 2002), and ASTER GDEM version-1 has an absolute vertical accuracy of 20 m at a 95% confidence level (ASTER GDEM Readme Handbook). The DEM data used for this study were downloaded from the Earth Explorer website (https://earthexplorer.usgs.gov/) on November 20, 2022.

To ensure data accuracy, elevation points collected during a field survey with a handheld GPS device (Garmin Montana 700) were used for validation. The geographic distribution of these elevation points within the basin is shown in Fig. 3. Data were collected in flat, open areas away from trees to minimize errors caused by poor GPS signal tracking. The GPS survey results were considered the most accurate data source of elevation data. Finally, the vertical accuracy of the

ASTER DEM was evaluated by comparing GPS control points with elevation data extracted from the DEM using the "Add Surface Feature" tool in ArcGIS 10.8. The Root Mean Square Error (RMSE) metric was used to assess the accuracy of the dataset.

Root Mean Square Error (RMSE)

When comparing fixed values, such as elevation points from GPS surveys, with estimated values like those from ASTER DEMs (Digital Elevation Models), the Root Mean Square Error (RMSE) is a commonly used statistic. RMSE quantifies the differences, or residuals, between these values and combines them into a single measure of accuracy (Congalton and Green, 2009; Ganie et al. 2023a). One of the key advantages of RMSE is its use of quadratic loss function, which amplifies the impact of larger errors on the final value. This property makes RMSE an effective tool for assessing the degree of uncertainty. In this context, RMSE analysis evaluates how closely the ASTER data align with the GPS survey data, with a lower RMSE indicating better agreement between the two datasets.

$$\mathrm{RMSE_V} = \sqrt{\frac{\sum_{i=1}^{n} (e_{vi})^2}{n}} \quad (1)$$

Where: e_{vi} is the vertical error, is equal to e_{oi}-e_{pi}; e_{pi} is the elevation of the i^{th} reference point on the DEM surface, and e_{oi} is the height of the i^{th} reference point above the mean sea level.

Since the vertical datum of the ASTER DEM is EGM96, and the Global Positioning System (GPS) typically calculates height based on the WGS84 vertical datum (Kaplan and Hegarty, 2006), the elevations from both datasets will differ for the same Ground Control Point (GCP) due to the discrepancy in vertical datums. To accurately compare GPS elevation data (based on WGS84) with ASTER elevation data, it is necessary to perform a vertical datum conversion, also known as datum matching (http://hydrosheds.cr.usgs.gov/hydro.php).

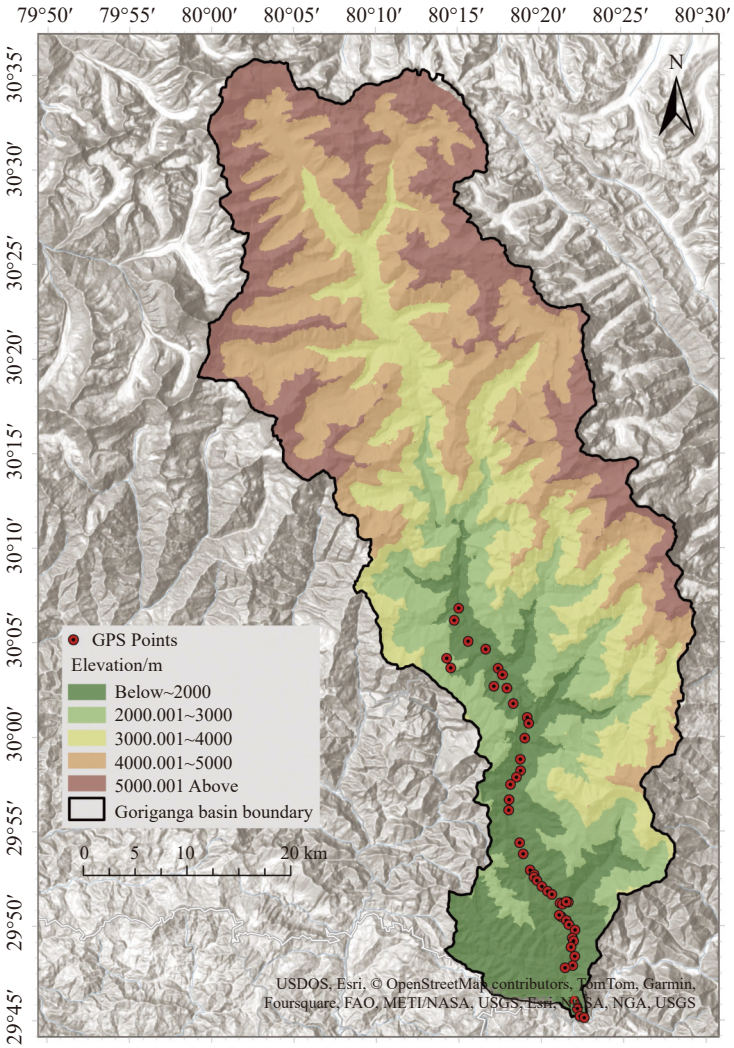

Fig. 3 Elevation based GCPS used for accuracy assessment

To address this issue of vertical datum discrepancies, GPS-based elevation points were converted to ellipsoidal heights as part of the geoid correction process. This conversion enables accurate comparison between the GPS and ASTER data. The transformation from ellipsoidal height to orthometric elevation is achieved using the following formula:

$$48H = h - N \quad (2)$$

Where: H is the orthometric height, h is the WGS84 ellipsoid height, N is the EGM96 geoid undulation.

The geoidal height information required for the DEM was calculated using the UNAVCO Geoid Height Calculator by entering the GPS latitude and longitude (UNAVCO facility. Geoid height calculator, accessed on August 23, 2024). This online tool provides the geoid height correction for a specific location on Earth, based on gravity models like EGM96 or EGM2008.

3 Methodology

To facilitate drainage delineation and subsequent analysis, topographic maps from the Survey of India, at a scale of 1:50,000, were employed. Key parameters, such as the total number of watersheds, stream segments, stream order, drainage pattern, as well as the length, perimeter, and area of the Goriganga drainage basin, were initially delineated using ASTER DEM data and then validated against the Survey of India topographical maps. The basin encompasses several Survey of India (SOI) map sheets, including 53N15, 62B2, 62B3, 62B4, 62B6, 62B7, 62B8, and 62C5 (Table 1). For the calculation of morphometric attributes within a Geographic Information System (GIS) framework, the aforementioned parameters are essential. These attributes include, but are not limited to, the bifurcation ratio, circulatory ratio, relief ratio, form factor, drainage density, stream frequency, overland flow, shape factor ratio, and form factor ratio. Each of these attributes was computed using their respective mathematical formulas.

Hydrogeological and aquifer maps of Uttarakhand were obtained from the India-WRIS platform (https://indiawris.gov.in/wris/, accessed on August 26, 2024). This map served as the primary data source for developing a detailed hydrogeological map of the Goriganga Basin. The process involved georeferencing the original map and clipping it to the boundaries of the Goriganga Basin using the clip tool in ArcPro 3.0. To further enhance the analysis, groundwater flow characterization for the study area were assessed by collecting groundwater depth measurements from eight handpumps distributed across the Goriganga Basin. These point locations were used as a basis for spatial analysis. To estimate groundwater depths at locations without measurements, spatial interpolation was performed using spherical kriging. Following interpolation, contours were generated at 1-meter intervals to provide a detailed topographic representation of the groundwater surface (Fig. 4).

3.1 Extraction of drainage network

In this research, the D8 (multi-directional method) was employed to delineate hierarchical orders within the drainage network. This approach utilized the hydrology tools in ArcGIS software applied to the ASTER Digital Elevation Model (DEM) with a resolution of 30 m (Morris and Heerdegen, 1988). To enhance the accuracy of the DEM, pixel-based errors such as sinks and peaks were corrected to address discontinuities within the drainage network. After refining the DEM, stream segments were delineated using Strahler's (1964) stream ordering system. A sequence of GIS operations was performed to map a highly accurate drainage network from the DEM. These operations included pixel filling, calculating flow direc-

Table 1 Details of data sources used for the study

S. No	Data	Specifications	Source
1.	ASTER DEM	Scene Id: ASTGTMV003_N29E080 ASTGTMV003_N30E079 (DOI):10.5067/ASTER/ASTGTM.003 Resolution -30m	United States Geological Survey (USGS) https://earthexplorer.usgs.gov/
2.	SOI toposheets	Toposheet numbers: 53N15, 62B2, 62B3, 62B4, 62B6, 62B7, 62B8, and 62C5. Scale: 1: 50,000	Survey of India (SOI) https://www.surveyofindia.gov.in/
3	Geology map	Shapefile	Bhukosh https://bhukosh.gsi.gov.in/Bhukosh/MapViewer.aspx accessed on 23.08.24.
4	Hydrogeological map	Tiff	India WRIS https://indiawris.gov.in/wris/, accessed on 26.08.24

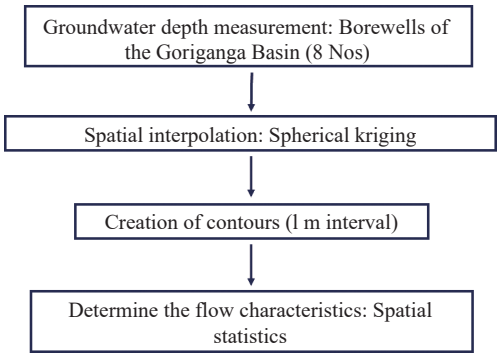

Fig. 4 Flowchart of the methodological framework for studying groundwater flow characteristics

tion and accumulation, and determining the contributing area from which water flows into an outlet grid cell (Tarboton and Baker, 2008). A threshold value of 200 was utilized to extract the drainage network from the DEM. The drainage pattern's accuracy was subsequently validated using the Survey of India topographical maps (Fig. 5).

3.2 Computation of morphometric parameters

To evaluate the intricate morphometric properties of the sub-basin, this study categorized the analysis into three fundamental dimensions: (1) Linear (2) areal and (3) relief characteristics. Each dimension was analysed using specific methodologies and mathematical equations, as outlined in Table 2. The Spatial Analyst Tool within ArcGIS 10.8 was employed to conduct a comprehensive analysis of the basin area's drainage density and its frequency distribution. The overall methodological framework for the study is depicted in Fig. 6.

4 Results

4.1 Accuracy assessment of ASTER Data

A set of 48 GPS-derived Ground Control Points (GCPs) was used to assess the accuracy of the ASTER DEM. While ASTER DEM references the EGM96 surface for elevation, the GPS system uses the WGS84 surface, a direct comparison between these elevation datasets was not feasible. To align the GPS-based ellipsoid heights with the EGM96 geoid reference surface, a transformation was performed using an online tool (available at https://www.unavco.org/software/geodetic-utilities/geoid-height-calculator/geoid-height-calculator.html, accessed on August 23, 2024). The transformed GPS heights were then compared with the ASTER heights (Fig. 7). The Root Mean Square Error (RMSE) for the ASTER DEM was calculated to be 9.26 m, which is significantly below the error threshold specified by the nodal agency and thus was deemed suitable for use in this study (ASTER GDEM Readme Handbook).

4.2 Hydrogeology of the Goriganga Basin

The hydrogeology of the Goriganga Basin is char-

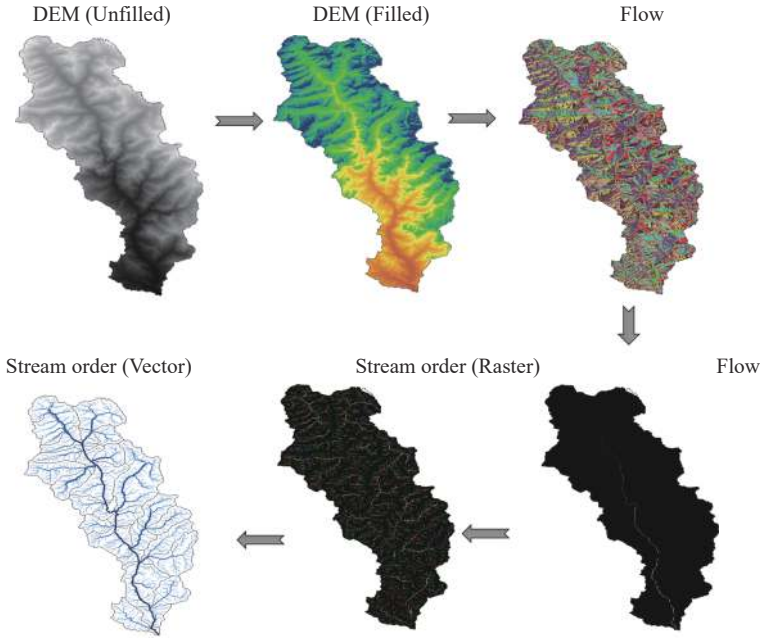

Fig. 5 Extraction of drainage layer of the study area

Table 2 The mathematical formulae adopted for the quantitative measurement of the morphometric parameters

Morphometric parameters	Symbol	Formula	References
Linear parameter measurement			
Basin length (km)	Lb	$1.312\times A^{0.568}$ Where: Lb = Basin length A = Basin area area (km^2)	Schumm (1956)
Stream number	Nu	Number of stream segments	Strahler (1952)
Stream order	U	Hierarchical rank	Strahler (1964)
Stream length (km)	Lu	Length of the stream segment	Horton (1945)
Mean stream length	Lsm	Lsm = Lu/Nu Where: Lsm = Mean stream length Lu = Total stream length of order 'u' Nu = Total no. of stream segments of order 'u'	Strahler (1964)
Stream length ratio	RL	RL = Lu/Lu-1 Where: RL = Stream length Lu = Total stream length of order 'u' Lu-1 = Total stream length of its next lower order	Horton (1945)
Bifurcation ratio	Rb	Rb = Nu/Nu+1 Where: Rb = Bifurcation ratio Nu = Total no. of stream segments of order 'u' Nu+1 = Number of stream segments of the next higher order	Schumm (1956)
Areal parameter measurement			
Basin area (km^2)	A	GIS software analysis	Schumm (1956)
Basin perimeter (km)	P	GIS software analysis	Schumm (1956)
Length of overland flow (km)	Lg	Lg = 1/D×2 Where: Lg = Length of over land flow D = Drainage density	Horton (1945)
Drainage density (km/km^2)	Dd	Dd = Lu/A Where: D = Drainage density Lu = Total stream length of order 'u' A = Area of the basin (km^2)	Horton (1932)
Stream frequency (km/km^2)	Fs	Fs = Nu/A Where: Fs = Stream frequency Nu = Total no. of streams of all orders A = Area of the basin (km^2)	Horton (1932)
Constant of channel maintenance (Km^2/Km)	C	C = 1/Dd Where: C = Constant of channel maintenance Dd =Drainage density	Schumm (1956)
Drainage intensity	Di	Di = Fs/Dd Where: Di = Drainage intensity Fs = Stream frequency Dd = Drainage density	Faniran (1968)
Infiltration number	If	If = Fs×Dd Where: If = Infiltration number Fs = Stream frequency Dd = Drainage density	Faniran (1968)
Texture ratio	Rt	Rt = N1/P	Schumm (1956)

Table 2 (continued)

Morphometric parameters	Symbol	Formula	References
		Where: Rt = Texture ratio	
		N1 = Number of 1st order streams	
		P = Basin perimeter (km)	
Drainage texture	Dt	Dt = Nu/P	Horton (1945)
		Where: Dt = Drainage texture	
		Nu = Total number of streams	
		P = Perimeter (km)	
Form factor	Ff	$Rf = A/Lb^2$	Horton (1932)
		Where: Rf = Form factor	
		A = Area of the basin (km^2)	
		Lb^2 = Square of basin length (km)	
Circulatory ratio	Rc		
		Rc = 4×Pi×A/P2	Miller (1953)
Circularity ratio	Rc		
		Where: Rc = Circulatory ratio	
		Pi ='Pi' value, i.e. 3.14	
		A = Area of the basin (km^2)	
		P = Perimeter (km)	
Elongation ratio	Re	Re = 2v(A/Pi/Lb)	Strahler (1957)
		Where: Re = Elongation ratio	
		Pi = 'Pi' value, i.e. 3.14	
		A = Area of the basin (km^2)	
		Lb = Basin length (km)	
Relief parameter measurement			
Height of basin mouth (km)	z	GIS analysis / DEM	
Maximum height of the basin (km)	Z	GIS analysis/DEM	
Total basin relief (km)	H	H = Z - z	Strahler (1952)
		Where: H= Total basin relief	
		Z = Maximum height of the basin (km)	
		z = Height of basin mouth (km)	
Relief ratio	Rh	Rh = H/Lb	Schumm (1956)
		Where: Rh = Relief ratio	
		H = Total relief of the basin (km)	
		Lb = Basin length (km)	
Relative relief	Rr	Rr = 100 H/P	Schumm (1956)
		Where: Rr = Relative relief	
		H = Total relief of the basin (km)	
		P = Perimeter (km)	
Ruggedness number	Rn	Rn = Dd×H	Strahler (1964)
		Where: Rn = Ruggedness number	
		Dd = Drainage density	
		H = Total basin relief (km)	

acterized by four primary rock types: Basement Gneissic Complex, Limestone, Schist, and Shale (Fig. 8). The Basement Gneissic Complex (orange), composed of crystalline gneiss, is characterized by low porosity and permeability, making it less effective as an aquifer (Clark, 1985; Gustafson

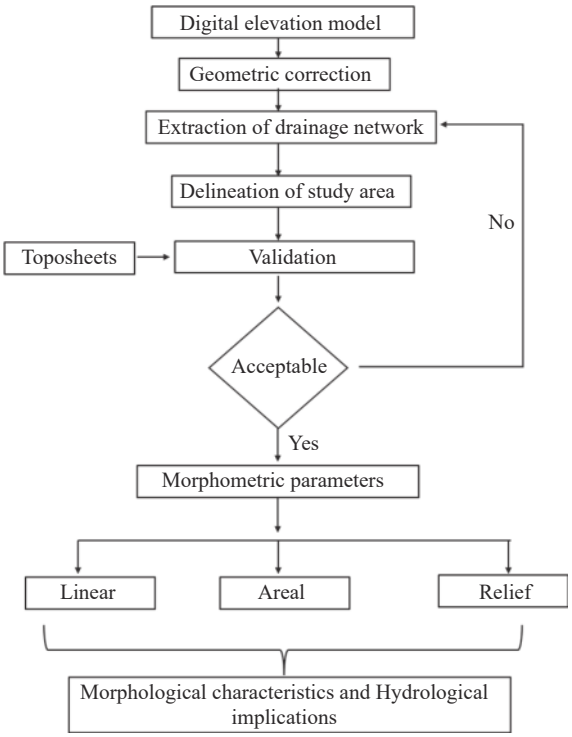

Fig. 6 Flowchart of the methodological framework used in the study

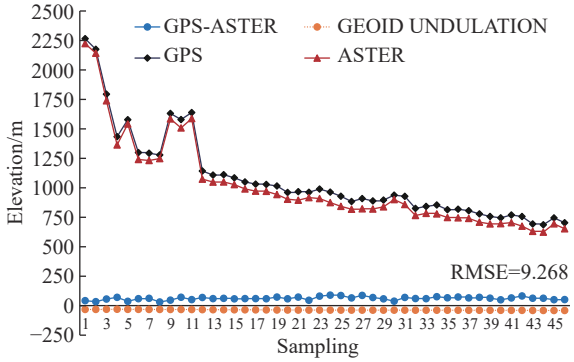

Fig. 7 Elevation and error values of ASTER DEM with respect to GPS vlaues

and Krásný, 1994). Groundwater storage and movement are predominantly confined to fractures, fault zones, or areas of extensive weathering. Schist (yellow), exhibits similar characteristics as Basement Gneissic Complex, wherein groundwater is stored and transmitted primarily through fractured and weathered zones. Conversely, Limestone regions (beige) have high potential for groundwater storage and flow due to their susceptibility to karstification (Kačaroğlu, 1999). This rock type typically forms highly permeable aquifers through the development of solution channels and conduits, facilitating rapid groundwater movement and storage. The karst systems are crucial in regions where water availability depends on the porosity and permeability of the subsurface lithology. Shale (blue), on the other hand, acts as an aquitard with its fine-grained, compact structure significantly impeding groundwater flow (Neuzil, 1994). Shale layers are typically impermeable and play a critical role in confining aquifers or protecting underlying groundwater resources from contamination.

4.3 Lithology

The Goriganga Basin is divided into two primary lithological units: Sediments and Meta-sediments (light pink) and Crystalline and Meta-sedimentary rocks (yellow) (Fig. 9). Each lithological unit exhibits distinct hydrogeological properties that influence groundwater occurrence and flow. The Sediments and Meta-sediments comprise a variety of rock types such as shale, quartzite, slate, phyllite, sandstones, dolomite, and limestone. These rock types typically form local or discontinuous aquifers (Hoek et al. 2005). The presence of limestone and dolomite in this unit suggests potential for karstification, which can enhance the permeability and storage capacity of the aquifers. However, the discontinuous nature of these aquifers implies that groundwater availability can be variable, heavily depending on the specific lithology and structural features like fractures and folds. On the other hand, the crystalline and metasedimentary rocks predominantly consist of gneissic complexes and associated intrusives. These rocks are typically less permeable due to their dense structure, which limits porosity (Lachassagne et al. 2021). As a result, the aquifers within this unit are generally localized and depend on secondary porosity developed through weathering and fracturing. Groundwater flow and storage are thus constrained to fractured zones and are less extensive compared to those in the sedimentary aquifers.

4.4 Morphometric characteristics

The morphometric parameters of the Goriganga River Basin were assessed using methodologies established by various scholars, tailored to the specific geographical context of the study area. The calculated outcomes for these parameters are systematically presented in Tables 3, 4, and 5. The total drainage area of the Goriganga River Basin encompasses an area of 2,183.11 km^2. The basin exhibits a drainage pattern that ranges from dendritic to sub-dendritic, shaped by the interplay

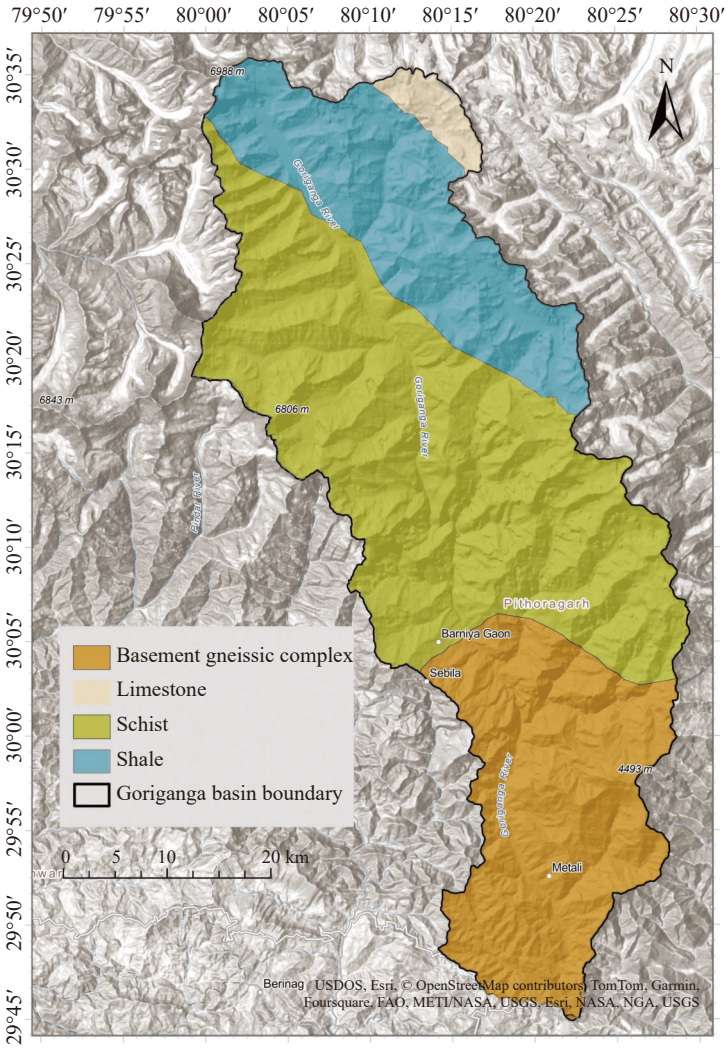

Fig. 8 Aquifer disposition of the Goriganga Basin

of topographical, geological, and meteorological conditions (Fig. 10). Regarding stream order classification, the basin is classified from 1st to 6th order (Table 3).

4.5 Linear morphometric parameters

Key linear parameters, such as basin length, stream order, stream number, stream lengths, mean stream length, stream length ratio, and bifurcation ratio, provide crucial insights into the structure of a drainage basin. Table 3 presents the calculated linear morphometric parameters for the Goriganga river basin.

Basin length, defined as the longest dimension parallel to the main drainage channel (Schumm, 1956), varies across the Goriganga Basin, with WS12 exhibiting the shortest basin length, while WS15 has the longest. The mean basin length across the Goriganga Basin is 13.57 km. Utilizing Strahler's stream ordering system (Strahler, 1964), the Goriganga Basin is classified as a 6th-order basin, with a total of 4,627 stream segments. The distribution of stream segments is as follows: WS115 has the highest number of segments (598), while WS12 has the fewest (10). Watersheds WS4, WS7, WS9, WS12, WS14, WS17, WS22, WS25, WS28, WS29, WS30, and WS32 are 6th-order, WS1, WS2, WS3, WS5, WS10, WS13, WS15, and WS26 are 5th-order, and WS6, WS8, WS11, WS16, WS18, and WS24 are 4th-order, as shown in Table 3 and Fig. 11.

Stream length is a critical parameter for evaluating drainage density and runoff contributions in sub-basins. The total stream length in the Goriganga basin is 3,648.30 km. First-order streams dominate this total, with a length of 2,073.61 km, indicating a broad distribution compared to higher-order streams (Table 3). Conversely, fifth-order streams have the smallest total length. WS15 has the longest total stream length, measuring 421.03 km, while WS32 has the shortest at 8.59 km. Mean stream length (Lsm) is calculated by dividing the

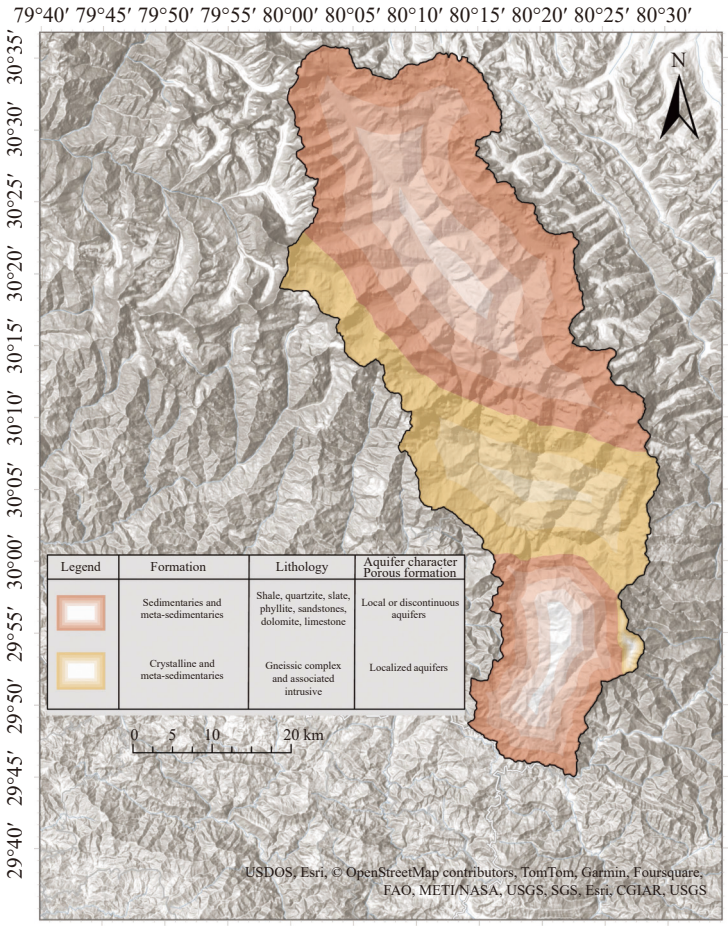

Fig. 9 Formation, lithology and aquifer characterization of Goriganga Basin

Table 3 Linear morphometric parameters characterization

Code	Basin length (Lb)	Stream order (U)						Stream No. 'Nu'	Stream length (Lu)						Total stream length
		1st	2nd	3rd	4th	5th	6th		Lu1	Lu2	Lu3	Lu4	Lu5	Lu6	
WS1	18.29	165	80	15	8	1		269	100.99	47.01	17.05	10.49	10.67		186.21
WS2	20.5	205	70	9	2	5		291	132.16	51.46	18.61	11.04	6.65		219.92
WS3	15.08	120	31	8	3	1		163	64.19	36.64	15.88	13.12	0.17		130.00
WS4	13.18	92	22	3	1	3	1	122	58.07	19.72	9.62	4.78	2.44	5.95	100.58
WS5	7.55	30	5	1		1		37	21.06	3.91	2.32		5.24		32.53
WS6	11.16	68	16	5	1			90	42.78	17.93	17.93	6.21			84.85
WS7	5.32	21	4	1	1		1	28	15.24	2.28	2.09	0.3		2.83	22.74
WS8	12.34	85	13	3	1			102	49.67	15.09	12.41	7.2			84.37
WS9	9.19	50	16	1		1	1	69	30.41	8.3	4.28		0.18	6.15	49.32
WS10	12.49	83	23	5	2	1		114	57.43	18.6	4.61	5.28	5.27		91.19
WS11	17.24	132	39	4	1			176	100.12	39.71	9.12	13.81			162.76
WS12	3.79	7			1	1	1	10	7.64			0.07	3.24	0.03	10.98
WS13	14.1	90	23	7	3	1		124	63.18	28.32	15.42	2.29	9.19		118.4
WS14	20.55	185	67	8	1	1	1	263	117.54	47.09	18.6	3.2	0.1	16.71	203.24
WS15	29.06	377	179	36	5	1		598	244.79	93.27	33.98	25.62	23.37		421.03
WS16	12.2	75	36	6	1			118	44.11	17.64	10.69	6.11			78.55
WS17	9.03	45	8	1			1	55	24.67	10.81	2.37			5.88	43.73

Table 3 (continued)

Code	Basin length (Lb)	Stream order (U)						Stream No. 'Nu'	Stream length (Lu)						Total stream length
		1st	2nd	3rd	4th	5th	6th		Lu1	Lu2	Lu3	Lu4	Lu5	Lu6	
WS18	11.55	70	15	6	1			92	38.26	18.09	7.43	7.91			71.69
WS19	12.37	68	33	4	3		1	109	49.8	18.99	3.95	6.57		6.66	85.97
WS20	15.53	122	35	6	2		1	166	81.3	28.04	8.3	11.3		6.68	135.62
WS21	18.19	167	57	10	4		1	239	103.28	37.46	15.94	9.43		10.86	176.97
WS22	12.42	89	21	5		1	1	117	49.71	19.63	6.14		10.4	0.27	86.15
WS23	14.19	87	26	7	16			136	64.9	30.26	4.8	12.59			112.55
WS24	15.94	102	57	3	1			163	74.9	35.95	13.58	7.53			131.96
WS25	7.85	22	4	1			1	28	24.72	7.07	3.16			4.94	39.89
WS26	4.28	14	2			1		17	4.94	1.85			2.88		9.67
WS27	20.31	181	72	5	1			259	105.48	41.36	30.15	9.94			186.93
WS28	22.86	187	59	9	1	1	1	258	123.84	56.41	25.6	6.2	0.83	21.37	234.25
WS29	16.16	93	51	7	1			152	73.87	28.63	12.82	12.31			127.63
WS30	11.99	66	26	3	1		1	97	48.62	25.85	7.57	1.74		9.26	93.04
WS31	15.56	98	51	3	1			153	51.23	34.63	9.12	12.01			106.99
WS32	3.85	9	1		1		1	12	4.71	0.08		0.1		3.7	8.59

Code	Mean stream length (Lsm)						Stream Length Ratio (Rl)					Bifurcation ratio (Rb)				
	Lu1/ N1	Lu2/ N2	Lu3/ N3	Lu4/ N4	Lu5/ N5	Lu6/ N6	Lu2/ Lu1	Lu3/ Lu2	Lu4/ Lu3	Lu5/ Lu4	Lu6/ Lu5	U1/ U2	U2/ U3	U3/ U4	U4/ U5	U5/ U6
WS1	0.61	0.58	1.13	1.31	10.67		0.47	0.36	0.62	1.02	-	2.06	5.33	1.88	8	
WS2	0.64	0.73	2.06	5.52	1.33		0.39	0.36	0.59	0.60	-	2.93	7.78	4.50	0.4	
WS3	0.53	1.18	1.98	4.373	0.17		0.57	0.43	0.83	0.01	-	3.87	3.88	2.67	3	
WS4	0.63	0.89	3.20	4.78	0.81	5.95	0.34	0.49	0.50	0.51	2.44	4.18	7.33	3.00	0.33	3
WS5	0.70	0.78	2.32		5.24		0.19	0.59	-	-	-	6.00	5.00		0	
WS6	0.62	1.12	3.58	6.21			0.42	1	0.35	-	-	4.25	3.20	5.00		
WS7	0.72	0.57	2.09	0.30		2.83	0.15	0.92	0.14	-	-	5.25	4.00	1.00		0
WS8	0.58	1.16	4.13	7.20			0.30	0.82	0.58	-	-	6.54	4.33	3.00		
WS9	0.60	0.51	4.28		0.18	6.15	0.27	0.52	0.00	-	34.17	3.13	16.00		0	1
WS10	0.69	0.80	0.92	2.64	5.27		0.32	0.25	1.15	1.00	-	3.61	4.60	2.50	2	
WS11	0.75	1.01	2.28	13.81			0.40	0.23	1.51	-	-	3.38	9.75	4.00		
WS12	1.09			0.07	3.24	0.03	0.00	-	-	46.29	0.0093			-	1	1
WS13	0.70	1.23	2.20	0.76	9.19		0.45	0.54	0.15	4.01	-	3.91	3.29	2.33	3	
WS14	0.63	0.70	2.32	3.2	0.1	16.71	0.40	0.39	0.17	0.03	167.1	2.76	8.38	8.00	1	1
WS15	0.64	0.52	0.94	5.12	23.37		0.38	0.36	0.75	0.91	-	2.11	4.97	7.20	5	
WS16	0.58	0.49	1.78	6.11			0.40	0.61	0.57	-	-	2.08	6.00	6.00		
WS17	0.54	1.35	2.37			5.88	0.44	0.22	0.00	-	-	5.63	8.00			0
WS18	0.54	1.20	1.23	7.91			0.47	0.41	1.06	-	-	4.67	2.50	6.00		
WS19	0.73	0.57	0.98	2.19		6.66	0.38	0.21	1.66	-	-	2.06	8.25	1.33		0
WS20	0.66	0.80	1.38	5.65		6.68	0.34	0.30	1.36	-	-	3.49	5.83	3.00		0
WS21	0.61	0.6	1.594	2.35		10.86	0.36	0.43	0.59	-	-	2.93	5.70	2.50		0
WS22	0.55	0.93	1.228		10.4	0.27	0.39	0.31	-	-	0.03	4.24	4.20		0	1
WS23	0.74	1.16	0.68	0.78			0.47	0.16	2.62	0.00	-	3.35	3.71	0.44		
WS24	0.73	0.63	4.52	7.53			0.48	0.38	0.55	0.00	-	1.79	19.00	3.00		
WS25	1.12	1.76	3.16			4.94	0.29	0.45	0.00	-		5.50	4.00			0

Table 3 (continued)

Code	Mean stream length (Lsm)						Stream Length Ratio (Rl)					Bifurcation ratio (Rb)				
	Lu1/ N1	Lu2/ N2	Lu3/ N3	Lu4/ N4	Lu5/ N5	Lu6/ N6	Lu2/ Lu1	Lu3/ Lu2	Lu4/ Lu3	Lu5/ Lu4	Lu6/ Lu5	U1/ U2	U2/ U3	U3/ U4	U4/ U5	U5/ U6
WS26	0.35	0.92			2.88		0.37	0.00	-		0.00	7.00			0	
WS27	0.58	0.57	6.03	9.94			0.39	0.73	0.33	0.00	-	2.51	14.40	5.00		
WS28	0.66	0.95	2.84	6.2	0.83	21.37	0.46	0.45	0.24	0.13	25.75	3.17	6.56	9.00	1	1
WS29	0.79	0.56	1.83	12.31			0.39	0.45	0.96	0.00	-	1.82	7.29	7.00		
WS30	0.73	0.99	2.52	1.74		9.26	0.53	0.29	0.23	0.00	-	2.54	8.67	3.00		0
WS31	0.53	0.67	3.04	12.01			0.68	0.26	1.32	0.00	-	1.92	17.00	3.00		
WS32	0.52	0.08		0.1		3.7	0.02	0	-	0.00		9.00		0.00		0

Table 4 Areal morphometric parameters

Code	A	P	Dd	Fs	C	Lg	Di	If	Rt	Dt	Rc	Re	Ff
WS1	103.38	54.04	1.8	2.6	0.56	1.11	1.44	4.69	3.05	4.98	0.31	0.44	0.63
WS2	126.45	50.84	1.74	2.3	0.57	1.15	1.32	4	4.03	5.72	0.3	0.61	0.62
WS3	73.65	39	1.77	2.21	0.57	1.13	1.25	3.91	3.08	4.18	0.32	0.61	0.64
WS4	58.12	39.8	1.73	2.1	0.58	1.16	1.21	3.63	2.31	3.07	0.33	0.46	0.65
WS5	21.8	21.05	1.49	1.7	0.67	1.34	1.14	2.53	1.43	1.76	0.38	0.62	0.7
WS6	43.32	31.01	1.96	2.08	0.51	1.02	1.06	4.07	2.19	2.9	0.35	0.57	0.67
WS7	11.75	16.16	1.94	2.38	0.52	1.03	1.23	4.61	1.3	1.73	0.42	0.57	0.73
WS8	51.73	35.54	1.63	1.97	0.61	1.23	1.21	3.22	2.39	2.87	0.34	0.51	0.66
WS9	30.76	29.39	1.6	2.24	0.62	1.25	1.4	3.6	1.7	2.35	0.36	0.45	0.68
WS10	52.83	32.34	1.73	2.16	0.58	1.16	1.25	3.72	2.57	3.53	0.34	0.63	0.66
WS11	93.18	46.08	1.75	1.89	0.57	1.14	1.08	3.3	2.86	3.82	0.31	0.55	0.63
WS12	6.48	12.01	1.69	1.54	0.59	1.18	0.91	2.61	0.58	0.83	0.45	0.56	0.76
WS13	65.38	38.22	1.81	1.9	0.55	1.1	1.05	3.43	2.35	3.24	0.33	0.56	0.65
WS14	126.95	58	1.6	2.07	0.62	1.25	1.29	3.32	3.19	4.53	0.3	0.47	0.62
WS15	233.65	80.04	1.8	2.56	0.55	1.11	1.42	4.61	4.71	7.47	0.28	0.46	0.59
WS16	50.7	32	1.55	2.33	0.65	1.29	1.5	3.61	2.34	3.69	0.34	0.62	0.66
WS17	29.84	26.55	1.47	1.84	0.68	1.36	1.26	2.7	1.69	2.07	0.37	0.53	0.68
WS18	46.01	31.4	1.56	2	0.64	1.28	1.28	3.12	2.23	2.93	0.35	0.59	0.66
WS19	51.96	35.15	1.65	2.1	0.6	1.21	1.27	3.47	1.93	3.1	0.34	0.53	0.66
WS20	77.5	41.91	1.75	2.14	0.57	1.14	1.22	3.75	2.91	3.96	0.32	0.55	0.64
WS21	102.42	46.21	1.73	2.33	0.58	1.16	1.35	4.03	3.61	5.17	0.31	0.6	0.63
WS22	52.3	35.15	1.65	2.24	0.61	1.21	1.36	3.69	2.53	3.33	0.34	0.53	0.66
WS23	66.13	38	1.7	2.06	0.59	1.18	1.21	3.5	2.29	3.58	0.33	0.58	0.65
WS24	81.22	48.04	1.62	2.01	0.62	1.23	1.24	3.26	2.12	3.39	0.32	0.44	0.64
WS25	23.34	23.31	1.71	1.2	0.59	1.17	0.7	2.05	0.94	1.2	0.38	0.54	0.69
WS26	8.02	11.56	1.21	2.12	0.83	1.66	1.76	2.56	1.21	1.47	0.44	0.75	0.75
WS27	124.35	55.29	1.5	2.08	0.67	1.33	1.39	3.13	3.27	4.68	0.3	0.51	0.62
WS28	153.09	57.72	1.53	1.69	0.65	1.31	1.1	2.58	3.24	4.47	0.29	0.58	0.61
WS29	83.16	40.56	1.53	1.83	0.65	1.3	1.19	2.81	2.29	3.75	0.32	0.63	0.64
WS30	49.2	34.93	1.89	1.97	0.53	1.06	1.04	3.73	1.89	2.78	0.34	0.51	0.66
WS31	77.78	43.64	1.38	1.97	0.73	1.45	1.43	2.71	2.25	3.51	0.32	0.51	0.64
WS32	6.66	11.14	1.29	1.8	0.78	1.55	1.4	2.32	0.81	1.08	0.45	0.67	0.76

Notes: A: Basin area; P: Perimeter; Dd: Drainage density; Fs: Stream frequency; C: Constant of channel maintenance; Lg: Length of overland flow; Di: Drainage intensity; If: Infiltration number; Rt: Texture ratio; Dt: Drainage texture; Rc: Circulatory ratio; Re: Elongation ratio; Ff: Form factor.

Table 5 Relief morphometric parameters

Code	Z	z	H	Rh	Rr	Rn	Code	Z	z	H	Rh	Rr	Rn
WS1	6	3.5	2.5	0.14	4.63	4.5	WS17	4.8	2.1	2.7	0.3	10.17	3.969
WS2	5.8	3.5	2.3	0.11	4.52	4.002	WS18	3.8	1.4	2.4	0.21	7.64	3.744
WS3	6.2	3.6	2.6	0.17	6.67	4.602	WS19	4.2	1.9	2.3	0.19	6.54	3.795
WS4	5.8	3.4	2.4	0.18	6.03	4.152	WS20	5.6	2.1	3.5	0.23	8.35	6.125
WS5	5.5	3.6	1.9	0.25	9.03	2.831	WS21	3.8	1.2	2.6	0.14	5.63	4.498
WS6	6	3.5	2.5	0.22	8.06	4.9	WS22	4	1.9	2.1	0.17	5.97	3.465
WS7	5.6	3.3	2.3	0.43	14.23	4.462	WS23	5.6	2	3.6	0.25	9.47	6.12
WS8	5.6	3.4	2.2	0.18	6.19	3.586	WS24	5.6	1.3	4.3	0.27	8.95	6.966
WS9	5.6	3.2	2.4	0.26	8.17	3.84	WS25	2.8	1.3	1.5	0.19	6.44	2.565
WS10	6	3.2	2.8	0.22	8.66	4.844	WS26	3	1.2	1.8	0.42	15.57	2.178
WS11	6.2	3.4	2.8	0.16	6.08	4.9	WS27	5.4	1.4	4	0.2	7.23	6
WS12	4.2	3.4	0.8	0.21	6.66	1.352	WS28	4	1	3	0.13	5.2	4.59
WS13	4.2	3.4	0.8	0.06	2.09	1.448	WS29	3.2	0.9	2.3	0.14	5.67	3.519
WS14	5.4	3.1	2.3	0.11	3.97	3.68	WS30	1.6	0.8	0.8	0.07	2.29	1.512
WS15	5.8	2	3.8	0.13	4.75	6.84	WS31	2	0.8	1.2	0.08	2.75	1.656
WS16	5.4	2.2	3.2	0.26	10	4.96	WS32	1.8	0.8	1	0.26	8.98	1.29

Notes: Z: Maximum Basin relief; z: Minimum basin relief; H: Total basin relief; Rh: Relief ratio; Rr: Relative relief; Rn: Ruggedness number.

total length of streams of a given order by the number of stream segments of that order. It provides insights into the spatial and hydrological characteristics of the stream network. Fifth-order streams exhibit the highest mean lengths, reflecting their extensive courses, while first-order streams, being shorter and more numerous, have the lowest mean lengths. Among the sub-basins, WS15 has the highest mean stream length, while WS26 has the lowest.

The stream length ratio, which compares the average length of streams of one order to that of the preceding order, reveals significant variations in stream length with increasing basin order. In the Goriganga basin, the highest ratios are between the 5^{th} and 4^{th} orders (46.25) and between the 6^{th} and 5^{th} orders (25.75), indicating substantial differences in stream lengths as order increases. This variability in stream length ratios across different orders is presented in Table 3.

The bifurcation ratio, introduced by Schumm (1956), is the ratio of the number of streams of a given order (Nu) to the number of streams in the next higher order (Nu+1). Notably, watersheds WS9, WS24, WS27, and WS31 exhibited higher bifurcation ratios between the 2^{nd} and 3^{rd} order streams, as detailed in Table 3. This suggests that local geological formations significantly influence the spatial organization and branching patterns of streams within these watersheds. Additionally, watersheds WS5, WS8, WS26, and WS32 showed elevated bifurcation ratios between the 1^{st} and 2^{nd} order streams, further highlighting the influence of geological characteristics on the drainage network.

4.6 Areal morphometric parameters

The areal characteristics of a drainage basin provide essential insights into its geological and climatic context, as well as its erosion history. These factors are critical for understanding the spatial arrangement, morphological features, hydrological behavior, and sedimentary processes within a drainage system. Key areal parameters, such as basin area, perimeter, circulatory ratio, and elongation ratio, quantitatively describe terrain dissection and geomorphological evolution.

The Goriganga River Basin has a total area of 2,183 km^2. Among the individual watersheds, WS15 is the largest, with an area of 233.65 km^2, while WS12 is the smallest at 6.482 km^2 (Table 4). The basin perimeter, delineating the boundary along watershed divides, measures 1,191.7 km. Individual watershed perimeter varies significantly from 11.14 km in WS32 to 80.04 km in WS15 (Table 4). The perimeter measurement is vital for assessing the basin's size, shape, and physical configuration (Schumm, 1956).

Horton proposed that the length of overland flow (Lg) could be approximated as half the inverse of the drainage density, reflecting its relationship with stream channel spacing. In the Gorig-

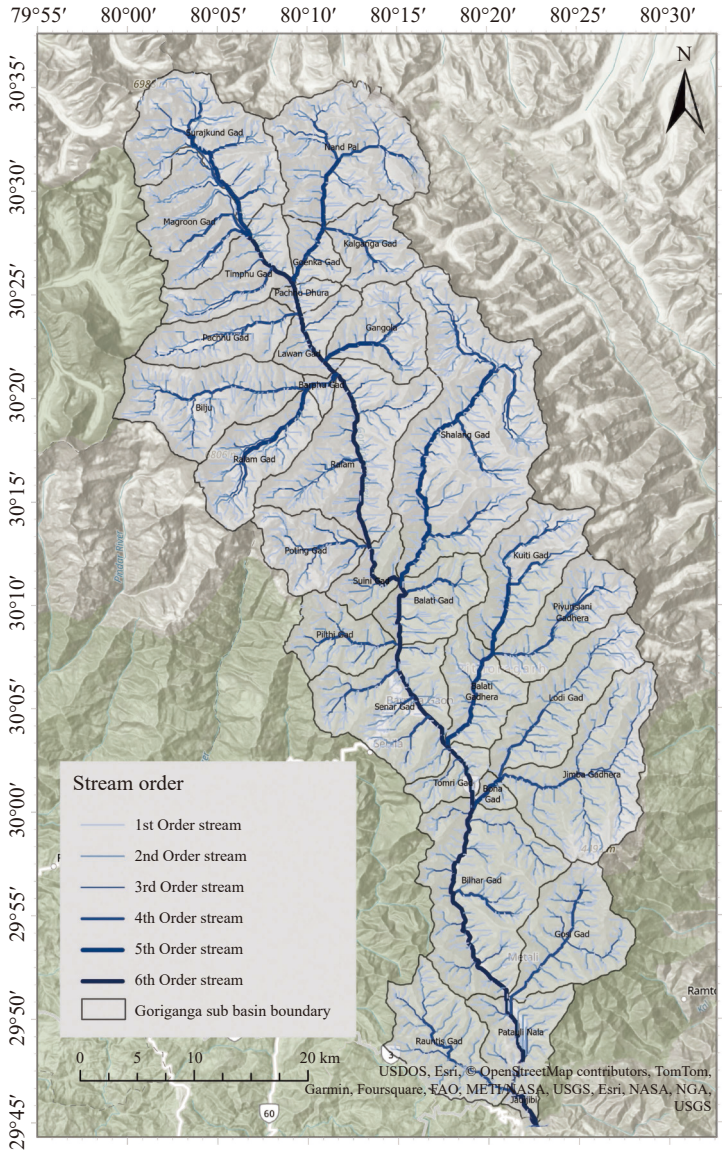

Fig. 10 Drainage pattern of the study area

anga basin, Lg values range from 1.02 km in WS6 to 1.66 km in WS26, indicating generally gentle slopes and extended flow paths across the watersheds (Table 4). Drainage density (Dd), representing the ratio of total stream lengths to basin area, measures the compactness of the stream network. Values in this study vary from 1.21 in WS26 to 1.96 in WS6, suggesting a predominantly coarse drainage texture (Horton, 1932; Strahler, 1964).

Stream frequency (Fs), which quantifies the total number of stream segments per unit area, ranges from 1.2 km^{-2} in WS25 to 2.6 km^{-2} in WS1. This variability reflects variability in the drainage network's texture and is influenced by the physical characteristics of the basin (Horton, 1932). Drainage texture (Dt), defined as the number of stream segments of all orders per unit area of basin perimeter, varies from 0.83 in WS12 (very coarse) to 7.47 in WS15 (very fine), highlighting the range of textural classifications within the basin (Horton, 1945). The constant of channel maintenance (C), indicating the area needed to support 1 km of channel, ranges from 0.51 in WS6 to 0.83 in WS26 (Table 4).

Drainage intensity, as defined by Faniran (1968), is the ratio of stream frequency (Fs) to Drainage density (Dd) and measures the hydrological aggressiveness of a basin. In the Goriganga basin, values ranged from 0.7 in WS25 to 1.76 in WS26, indicating varying susceptibility to erosion based on the characteristics of the drainage network (Table 4). The infiltration number, calculated as the product of drainage density (Dd) and stream frequency (Fs), varies from 2.05 in WS25 to 4.69 in WS1, reflecting a range from moderate to high infiltration capacities (Subayani

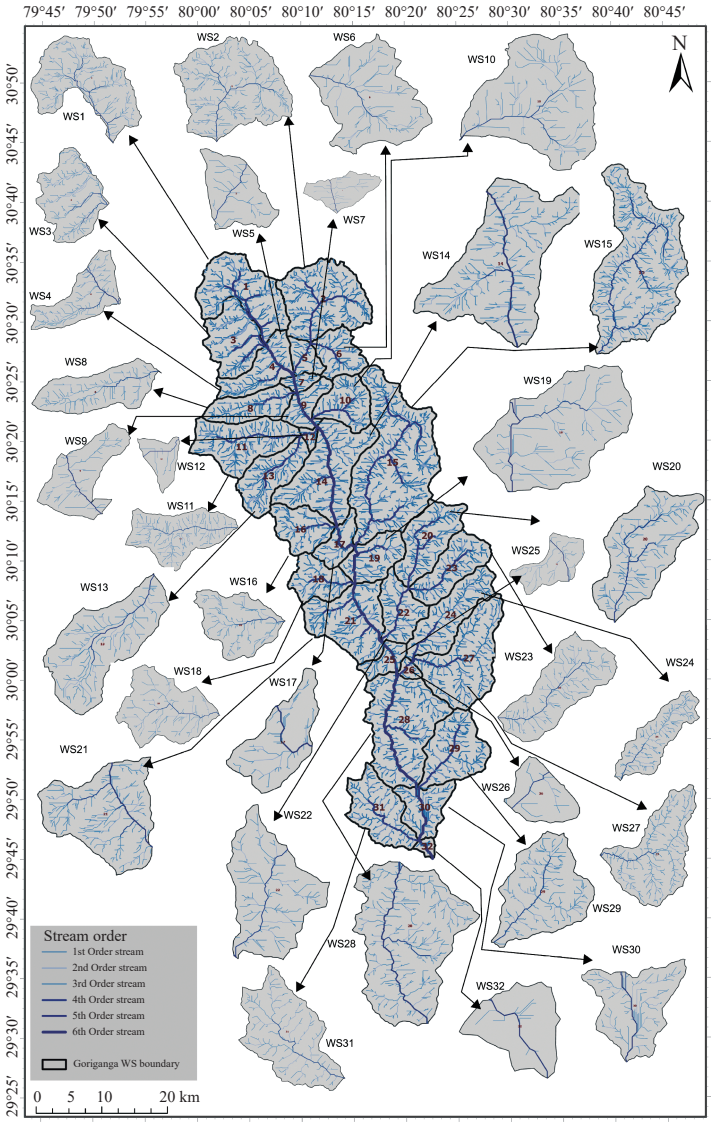

Fig. 11 Subwatersheds of the Goriganga Basin

et al. 2012). The texture ratio (Rt), representing the ratio of first-order streams to the basin perimeter, ranged from 0.58 in WS12 to 4.71 in WS15, highlighting differences in drainage texture (Schumm, 1956).

The Form factor (Ff), the ratio of basin area to the square of its length, ranged from 0.28 in WS15 to 0.45 in WS12, suggesting an overall elongated basin shape with flatter hydrograph characteristics conducive to flood management (Horton, 1945; Sreedevi et al. 2009). The circulatory ratio (Rc), which measures how closely the basin's shape approximates a circle compared to a basin with the same perimeter, ranged from 0.44 in WS1 and WS24 to 0.75 in WS26 (Miller, 1953; Strahler, 1964). The elongation ratio (Re), defined as the ratio of the diameter of a circle with the same area as the basin to the basin's maximum length, ranged from 0.59 in WS15 to 0.76 in WS12 and WS32, indicating morphologies from elongated to less elongated (Schumm, 1956).

4.7 Relief morphometric parameters

Relief morphometric parameters provide insights into the topographical gradient and overall terrain of a drainage basin. Key relief metrics include basin relief, relief ratio, relative relief, and ruggedness number. Basin relief (H), which represents the vertical distance between the highest and lowest points within a basin (Fig. 12), ranges from 0.8 km in watersheds WS12, WS13, and WS30 to 4.3 km in watershed WS24 (Table 5). The relief ratio (Rh), calculated as the ratio of vertical relief to the horizontal extent along the main drainage axis (Schumm, 1956), varies from 0.06 in watershed WS13 to 0.43 in watershed WS7 (Table 5). Relative relief (Rr) is computed as the vertical distance

from the highest point on the basin's perimeter to the stream outlet, with values ranging from 2.09 in watershed WS13 to 15.57 in watershed WS26 (Table 5). The Ruggedness number (Rn), which combines slope steepness and extent, is determined as the product of basin relief and drainage density (Strahler, 1957). Rn values in the study range from 1.29 in WS32 to 6.9 in WS24 (Table 5).

5 Discussion

5.1 Linear Morphometric parameters

Lithological and structural factors significantly influence the configuration of drainage basins, as evidenced by linear characteristics, which are crucial for analyzing river and tributary dynamics. In the Goriganga Basin, the assessment of watershed lengths revealed that watersheds with the highest stream counts, such as 1, 2, 3, 4, 8, 10, 11, 13, 14, 15, 16, 19, 20, 21, 22, 23, 24, 27, 28, 29, and 31, are characterized by greater permeability and higher erosion susceptibility (Moharir et al. 2021). This observation aligns with Horton's laws (Horton, 1945), which state that first-order streams are the most common, with their numbers decreasing in higher orders.

Notable exceptions include such as WS2 and WS4, which have more 5th-order streams than 4th-order streams, and WS23, where 4th-order streams outnumber 3rd-order streams. These deviations align with Horton's laws and Strahler's (1964) stream ordering system. The basin's uneven slope gradient, resulting in fewer streams of higher order, suggests significant tectonic activity (Nikhilraj et al. 2012).

Variation in stream lengths across different orders reflects a complex interplay of geomorpho-

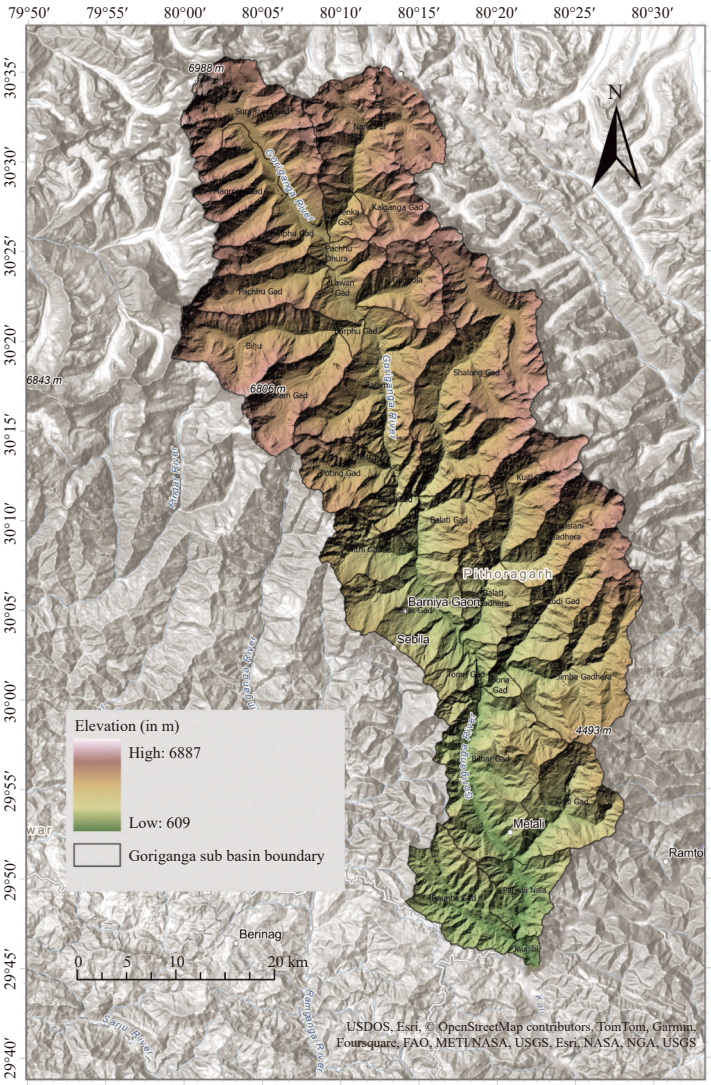

Fig. 12 Elevation profiling of Goriganga Basin

logical and hydrological factors, including altitude gradient, lithology, and slope steepness. The predominance of first-order streams, which contribute significantly to the total stream length, highlights their role in shaping the drainage network's structure (Table 3). This variation also indicates differences in basin relief (Vyas et al. 2020) and is influenced by geomorphological maturity and landscape evolution through erosion and sedimentation dynamics (Philips, 2006).

Horton's law of stream length, which suggests that average stream length increases with stream order, generally applies to the Goriganga Basin's watersheds up to the 4th order (Table 3). However, in this basin, the 6th-order streams exceed 5th-order streams in length, suggesting higher hydraulic conductivity for the 6th-order streams (Mohammed, 2020). Typically, mountainous and plateau environments exhibit lower mean stream length ratios, whereas plains show higher ratios. Shrestha et al. (2017) note that mean stream length generally increases with stream order. Nevertheless, anomalies in the Goriganga Basin reveal that 6th-order streams exhibit longer mean lengths than expected, indicating ongoing channel-lengthening processes that are not observed in subsequent orders (Singh and Singh, 1997).

Nag and Chakraborty (2003) observed that channel segments of a given order are longer than those of the immediate lower order but shorter than the next higher order, reflecting the impact of uniform geological weathering and erosion. Deviations from this pattern in watersheds 12, 13, 19, 20, 23, and 31 suggest irregular catchment development. Sreedevi et al. (2009) found that variations in slope and topography affect stream length ratios between successive stream orders, with these ratios closely related to surface flow discharge and the basin's erosional stage. The stream length ratio reflects the basin's hydrological behaviour (Kabite and Gessesse, 2018).

Thomas et al. (2010) suggested that an increasing stream length ratio from lower to higher orders indicates geomorphic maturity, while deviations from this trend imply that geomorphic evolution is still in the early stages (Sreedevi et al. 2009). The “Rl” values for the Goriganga Basin indicate geomorphic maturity (Table 3), and variations in “Rl” across different stream orders highlight uneven topography and differences in infiltration rates.

The bifurcation ratio, which reveals the branching pattern of a river system, is essential for understanding the influence of geological structures on drainage networks. In the Goriganga Basin, the mean bifurcation ratio is 3.14, indicating moderate branching. The bifurcation ratios vary from 0.1 to 5.00 across different watersheds, reflecting varying geological controls. Lower ratios suggest more uniform and less constrained branching, potentially due to homogeneous lithology or minimal structural influences, consistent with Strahler's (1964) findings. Additionally, Giusti and Schneider's (1965) hypothesis that bifurcation ratios decrease with increasing stream order is supported by the Goriganga basin data (Table 3).

5.2 Areal morphometric parameters

Areal parameters of a drainage basin, including lithology, geological structure, climate, and denudation history, significantly influence the spatial arrangement, geometry, and discharge characteristics of drainage systems. There is an inverse relationship between discharge per unit area and basin size (Chorley et al. 1957). Key morphometric variables, such as area (A), perimeter (P), and length (Lb), are essential for understanding watershed spatial characteristics (Horton, 1932). The variability in basin area underscores the heterogeneity within the Goriganga Basin.

The "length of overland flow" (Lg), as defined by Horton (1945), measures the distance that rainwater travels across the land before entering stream channels. There is an inverse relationship between terrain gradient and "Lg", meaning that lower relief leads to longer overland flow paths, while higher relief results in shorter paths (Kumar et al. 2020). Olszevski et al. (2011) observed that small "Lg" values during heavy rainfall increase the risk of flooding due to reduced water absorption capacity. In the Goriganga Basin, the moderate "Lg" values suggest that rainfall takes longer to reach the streams, with significant flow occurring primarily during major rainfall events. This extended lag period reduces the likelihood of flash floods. Chorley (1957) states that lower "Lg" values can lead to increased runoff and higher stream discharge. Consequently, the findings indicate that the watersheds in the Goriganga Basin are likely to experience moderate surface runoff and stream discharge during intense rainfall events.

Smith (1950) classified drainage densities into categories, ranging from very coarse (Dd < 2) to very fine (Dd > 8), each affecting drainage efficiency and erosional dynamics differently. In this study, the Goriganga Basin's coarse drainage texture suggests that the area is underlain by resistant and permeable subsurface materials (Table 4).

Literature indicates that low drainage density is often linked to resistant or porous sub-soil, dense vegetation, and low topographical relief (Nag, 1998). In contrast, high drainage density usually reflects less permeable substrates, sparse vegetation, and more pronounced relief. Strahler (1952) states that high drainage density is associated with fine drainage textures, increased runoff, and higher erosion potential, while low drainage density corresponds to coarse drainage textures. Further, higher drainage density regions often tend to have poor groundwater prospects than the lower drainage density regions (Muthamilselvan et al. 2019) Thus, the Goriganga Basin's low drainage density suggests a balanced interaction between vegetative cover and sub-soil permeability, contributing to the region's hydrological and geomorphological stability.

Stream frequency reflects the structural and textural characteristics of a drainage network, with higher values indicating a denser system (Ganie et al. 2023c). There is a direct correlation between stream frequency and drainage density, suggesting that increased drainage density leads to a greater number of stream channels. This correlation points to varying infiltration capacities across watersheds, with WS1 and WS15 exhibiting lower infiltration capabilities compared to WS25, which has the highest infiltration capacity (Pankaj and Kumar, 2009; Ganie et al. 2024). The relationship between stream frequency and drainage density underscores the influence of drainage density on stream numbers and the impact of geomorphological factors such as slope and geological structures on stream lengths (Horton, 1945). In the Goriganga Basin, Dt values indicate that watersheds with very coarse drainage textures, including WS5, WS7, WS12, WS25, WS26, and WS32, experience the longest hydrological basin lag times. These are followed by coarse, fine, and very fine textures (Esper, 2008). This variation in drainage texture reflects differing durations to peak flow, with WS12 having the longest and WS15 the shortest, highlighting the complex relationship between drainage texture and watershed hydrology.

Areas with lower "C" values typically exhibit features such as higher drainage density, impervious rock types, and dense forest cover (Ganie et al. 2022). In the Goriganga Basin, the "C" values reflect high surface permeability and dense vegetation across the watersheds. The minimal variation in "C" values among the watersheds suggests relatively uniform geological and vegetative characteristics (Ganie et al. 2023b).

The infiltration number (If) represents a watershed's capacity for water infiltration, with a direct relationship to runoff and an inverse relationship to the basin's infiltration capacity. Higher "If" values signify reduced infiltration and increased runoff, whereas lower "If" values indicate greater infiltration and reduced runoff (Faniran, 1968). The "If" results for the Goriganga Basin support these findings and reveal variability in infiltration and runoff characteristics, highlighting the need for tailored water resource management and erosion control strategies within the basin.

The texture ratio (Rt) provides insights into a basin's geological characteristics, infiltration capacity, and terrain relief. In the Goriganga Basin, Rt values range from 0.58 in WS12 to 4.71 in WS15. These values suggest that WS15, with a higher Rt, is likely to experience a longer basin lag time compared to WS12, which is expected to have a shorter lag time. This variation highlights the significant impact of the basin's physical and geological attributes on its hydrological response.

The form factor (Ff) is crucial for assessing a basin's flow intensity and morphological shape. Lower "Ff" values indicate a more elongated basin shape, associated with less intense peak flows that are sustained over a longer duration. In contrast, higher "Ff" values suggest a more circular basin shape, which typically experiences shorter but more intense flood flows (Howard, 1990). The relatively low "Ff" values observed in the watersheds of the Goriganga Basin (Table 4) indicate that these watersheds have elongated shapes, leading to more prolonged and manageable hydrographs compared to basins with more circular basins.

The circulatory ratio (Rc) is a key metric for assessing the effectiveness of a basin's drainage system and its geological consistency. It also reflects the extent of tectonic influence, as discussed by Vinutha and Janardhana (2014). Basins with low "Rc" values tend to experience minimal structural disturbances, while higher values indicate more significant disturbances. According to Miller (1953), an Rc range of 0.4 to 0.7 characterizes elongated basins with homogeneous, highly permeable geological substrates. Additionally, "Rc" provides insight into the evolutionary phase of the tributary watershed: Lower values represent youth, intermediate values denote maturity, and higher values signify an advanced stage (Wilson et al. 2012). The "Rc" values observed for the Goriganga Basin align with Miller's categorization, indicating a predominantly elongated basin with low surface runoff and permeable subsoil, characteristic of a youthful

developmental stage. This highlights the basin's geomorphological and hydrological features, suggesting it is in an early phase of fluvial evolution.

The elongation ratio (Re) classifies watersheds based on their general slope, categorizing them into circular (0.9–1.0), oval (0.8–0.9), less elongated (0.7–0.8), elongated (0.5–0.7), and highly elongated (below 0.5). Hydrologically, more elongated basins are less efficient in runoff discharge compared to circular basins due to the longer travel path of water, which enhances infiltration and interaction with the basin surface (Singh and Singh, 1997).

In the Goriganga Basin, watersheds WS1, WS4, WS10, WS14, WS15, and WS24, with Re values below 0.5, exhibit highly elongated shapes. In contrast, most other watersheds have Re values between 0.5 and 0.7, indicating a less elongated morphology. Given that the majority of watersheds in the basin fall within the 0.6 to 0.8 range, they are relatively less susceptible to soil erosion due to their moderate gradients and relief, compared to the more elongated watersheds (Reddy et al. 2004).

5.3 Relief morphometric parameters

Relief morphometric parameters are critical for understanding erosion and mass movement processes that shape landscapes and for examining denudational dynamics. High relief basins, characterized by steep slopes, generally experience significant weathering processes rather than hillslope movements, leading to high-velocity surface runoff and reduced infiltration, as observed in watersheds WS15, WS16, WS20, WS23, WS24, WS27, and WS28. In contrast, watersheds with lower relief, such as WS12, WS13, WS30, WS31, and WS32, show greater weathering and higher infiltration rates, reflecting a complex interplay of physical processes across the basin.

The relief ratio (Rh) measures the overall gradient or steepness of a drainage basin, serving as an indicator of erosional intensity. Larger drainage areas and sub-watersheds typically have lower "Rh" values, highlighting a negative correlation between basin size and relief (Gottschalk, 1964). The high Rh values across all watersheds indicate elevated erosion intensity, consistent with findings from the Geological Survey of India (GSI, 1981) and Mahadevaswamy et al. (2011), which link geological substrates to topographical features. Relative relief, as highlighted by Gayen (2013), is a key morphometric parameter for evaluating terrain morphology. It is defined as the elevation difference between the highest and lowest points within a given area (Mustak, 2012). Watersheds such as WS13, WS30, and WS31 have lower relative relief, suggesting reduced runoff and soil erosion. Conversely, watersheds with relative relief values between 3 and 16 exhibit higher relief, indicating a greater potential for surface runoff and soil erosion. This variation demonstrates the significant relationship between terrain morphology and hydro-geomorphological processes (Aher et al. 2014; Ganie et al. 2024).

The Ruggedness Number (Rn) measures the topographical roughness or undulation within a basin (Selvan et al. 2011) and reflects the structural complexity of landforms and their susceptibility to erosion (Vijith and Satheesh, 2006). "Rn" values range from 0 to 1, with lower values indicating smoother surfaces and higher values indicating increased ruggedness. The results reveal that the watersheds within the Goriganga Basin are generally smooth. Strahler (1964) noted that "Rn" increases with rising drainage density and relief, which is indicative of steep and elongated slopes. The "Rn" values for the Goriganga Basin suggest a moderate susceptibility to soil erosion, highlighting the interplay between topographical features and erosion potential.

5.4 Hydrogeological and aquifer characteristics of the basin

The aquifer disposition within the Goriganga Basin reveals a diverse and complex hydrogeological setting, heavily influenced by the region's lithological characteristics. The primary aquifer system in the basin is composed of limestone, known for its high permeability and karstic features. These limestone areas exhibit substantial groundwater potential, allowing for significant water storage and rapid flow. However, the vulnerability of limestone aquifers to contamination, particularly in unconfined settings, warrants careful groundwater management practices. On the other hand, the Basement Gneissic Complex and Schist regions exhibit limited aquifer potential, with groundwater primarily confined to structurally controlled zones. Shale, acting as a confining layer or aquitard, plays an essential role in preventing vertical water movement and shielding aquifers from potential surface contamination. This geological heterogeneity implies that groundwater availability and movement are highly localized within the basin.

The hydrogeology of the Goriganga Basin

reveals significant variability in aquifer potential across different geological units within the basin. Sedimentary and Meta-sedimentary units offer moderate groundwater potential, with local or discontinuous aquifers that are likely to yield variable amounts of water. The inclusion of carbonate rocks, such as limestone and dolomite, enhances the potential for karst aquifers, which can provide significant localized groundwater flow. However, these aquifers are also more susceptible to contamination due to their high permeability and the rapid movement of water through karst features. On the other hand, the Crystalline and Meta-sedimentary units provide limited groundwater storage, predominantly through fractures or weathered zones. These localized aquifers are crucial in areas lacking sedimentary aquifers but generally provide lower and more sporadic yields. The hydrogeological system within the basin is thus highly heterogeneous, with groundwater availability and movement strongly influenced by lithological variations, structural geology, and weathering processes. Consequently, effective groundwater management in the Goriganga basin will require localized strategies that consider the specific characteristics and capacities of each lithological unit.

5.5 Groundwater flow characterization

In the present study, eight handpumps were examined to conceptualize the groundwater flow characteristics (Fig. 13). The movement of groundwater is primarily influenced by geological factors such as lithology, discontinuities, and structural formations (Lü et al. 2020). Handpumps HP1 and HP2 are situated within a granite and granodiorite complex, which includes gneiss rocks. In these areas, groundwater flow is significantly influenced by fractures that enhance secondary porosity and permeability, leading to groundwater occurrence in semi-confined or unconfined conditions within the gneiss. The high frequency of fractures in this rock mass contributes to greater transmissivity and permeability, facilitating groundwater movement. HP3 is located near a thrust/fault zone where quartzite alternates with limestone formations. In this setting, groundwater is found in unconfined to semi-unconfined conditions, with water transmission occurring through discontinuity planes. The perched water table in this geological context is significant, and groundwater flow is strongly influenced by the orientation and frequency of structural discontinuities.

In HP4, groundwater flows through limestone and dolomitic terrains, where its movement is primarily controlled by structural discontinuities, including folds and faults. HP5 is situated in the Rautgara Formation, predominantly composed of quartzite, and bounded by two fault zones. The geological characteristics of this area-highly sheared, fractured, and jointed rock mass-result in elevated water conductivity and the presence of perched water tables. For HP6, HP7, and HP8, the underlying rock mass consists mainly of phyllite and schist. In these locations, groundwater is semi-confined, with its movement governed by fractures, shear zones, and structural features. HP7 and HP8 are located near thrust zones, where groundwater conductivity is further influenced by numerous shear zones, fractured rock masses, and the frequent folding. These structural featurs significantly impact groundwater availability and flow dynamics in these areas.

6 Conclusions

(1) The Goriganga River Basin is predominantly characterized by lower-order streams, particularly first-order streams, exhibiting a dendritic to sub-dendritic drainage pattern. This pattern suggests a relatively uniform lithological composition across the basin. There is a positive correlation between drainage density and the number of stream channels across various sub-watersheds, reflecting variations in topography and geomorphology. These variations influence stream frequency and bifurcation ratios, potentially indicating the presence of geological discontinuities within the basin.

(2) The basin's relatively low drainage density and moderate relief enhance infiltration and increase groundwater potential, resulting in minimal surface runoff. The presence of highly permeable subsoils further contributes to efficient groundwater recharge processes. Groundwater availability within the basin is closely linked to its lithological heterogeneity. Limestone, characterized by high permeability and karstic features, serves as the primary aquifer, offering substantial groundwater reserves, although its high permeability also heightens contamination risk. In contrast, shale, acts as a confining layer, and the fractured zones of the Gneissic and Schist regions provide limited groundwater storage.

(3) Morphometric analysis of the basin reveals a range of shapes from elongated to less elongated forms. These variations in basin shape significantly influence infiltration rates and hydrological responses. The morphological diversity directly affects surface runoff, sediment transport, and the overall availability of water resources.

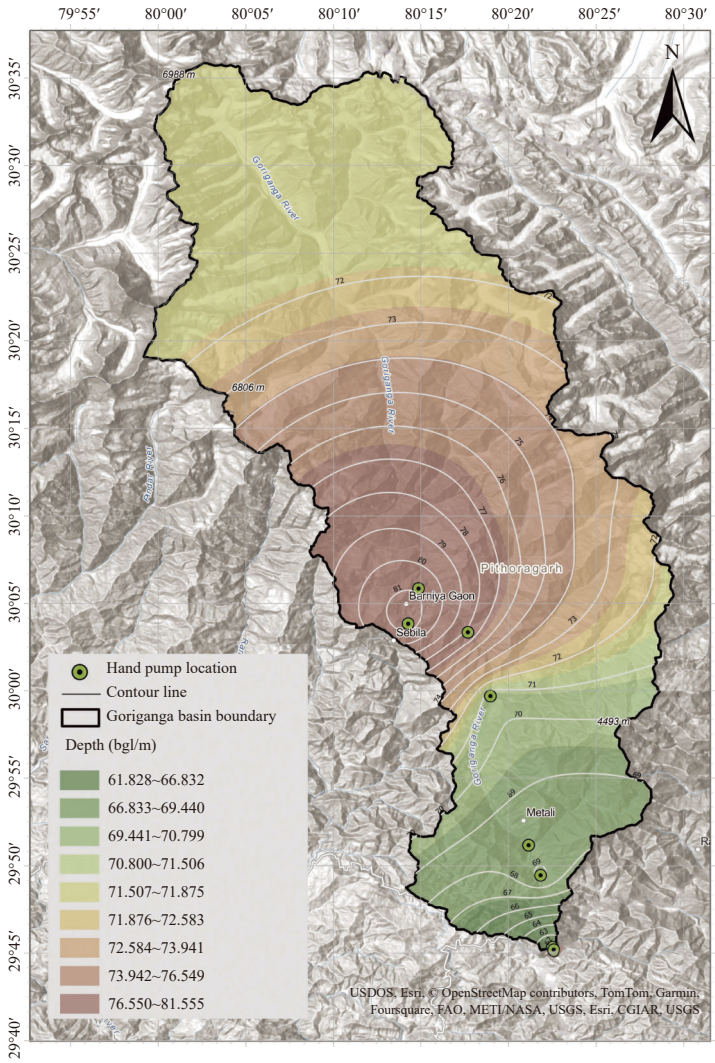

Fig. 13 Groundwater flow characterization of Goriganga Basin

(4) The application of morphometric analysis techniques is critical for evaluating river basins, providing essential insights into soil and water conservation and supporting the sustainable management of natural resources. These techniques offer valuable guidance for policymakers and decision-makers engaged in river basin management and hydrological planning. By emphasizing the importance of understanding each basin's specific geomorphological and lithological characteristics, morphometric analysis ensures more effective and tailored resource management strategies.

References

Abijith D, Saravanan S, Singh L, et al. 2020. GIS-based multi-criteria analysis for identification of potential groundwater recharge zones - a case study from Ponnaniyaru watershed, Tamil Nadu, India. Hydrological Research, 3: 1−14. DOI：10.1016/j.hydres.2020.02.002.

Abrams M, Hook S, Ramachandran B. 2002. ASTER User Handbook Version 2. Jet Propulsion Laboratory, 4800: 135.

Aher PD, Adinarayana J, Gorantiwar SD. 2014. Quantifcation of morphometric characterization and prioritization for management planning in semi-arid tropics of India: A remote sensing and GIS approach. Journal of Hydrology, 511: 850−860. DOI：10.1016/j.jhydrol.2014.02.028.

Ashok K. 2014. Studies on Ichthyofaunal Diversity with special reference to monthly and seasonal variations of fish landings in glacial fed Mountainous Goriganga River of Kumaun Himalaya, Uttarakhand, India. Research Journal of Animal, Veterinary and Fishery Sciences, 2(4): 1−12.

ASTER G. 2011. Validation Team: ASTER global digital elevation model version 2–summary of validation results. NASA Land Processes Distributed Active Archive Center and Joint Japan-US ASTER Science Team, 435.

Chorley RJ. 1957. Climate and morphometry. The Journal of Geology, 65(6): 628−638. DOI：10.1086/626468.

Clark L. 1985. Groundwater abstraction from basement complex areas of Africa. Quarterly Journal of Engineering Geology and Hydrogeology, 18(1): 25−34. DOI：10.1144/GSL.QJEG.1985.018.01.05.

Congalton RG, Green K. 2009. Assessing the accuracy of remotely sensed data - Principles and practices. Second edition. CRC Press, Taylor & Francis Group, Boca Raton, FL 978-1-4200-5512-2.

Das PK. 2015. Global warming, glacial lakes and cloud burst events in Garhwal-Kumaon Himalaya: A hypothetical analysis. International Journal of Environmental Sciences, 5(4): 697−708. DOI：10.6088/ijes.2014050100065.

Esper Angillieri MY. 2008. Morphometric analysis of Colangüil River Basin and flash flood hazard, San Juan, Argentina. Environmental Geology, 55(1): 107−111. DOI：10.1007/s00254-007-0969-2.

Faniran A. 1968. The index of drainage intensity: A provisional new drainage factor. Australian Journal of Science, 31(9): 326−330.

Ganie PA, Posti R, Pandey PK. 2024. Exploring and modelling the hydro-morphological landscape of a Himalayan basin: A geospatial study of Nandakini Basin in Uttarakhand, India. Discover Geoscience, 2(1): 27. DOI：10.1007/s44288-024-00032-2.

Ganie PA, Posti R, Aswal AS, et al. 2023a. A comparative analysis of the vertical accuracy of multiple open-source digital elevation models for the mountainous terrain of the north-western Himalaya. Modeling Earth Systems and Environment, 9(2): 2723−2743. DOI：10.1007/s40808-022-01641-x.

Ganie PA, Posti R, Bharti VS, et al. 2023b. Striking a balance between conservation and development: A geospatial approach to watershed prioritisation in the Himalayan Basin. Conservation, 3(4): 460−490. DOI：10.3390/conservation3040031.

Ganie PA, Posti R, Kumar P, et al. 2016. Morphometric analysis of a Kosi River Basin, Uttarakhand using geographical information system. International Journal of Multidisciplinary and Current Research, 4: 1190−1200.

Ganie PA, Posti R, Kunal G, et al. 2024a. Principle and applications of Geographic Information System (GIS) in coldwater fisheries development in India. In: Sarma D, Chandra S, Mallik SK. (eds) Aquaculture and Conservation of Inland Coldwater Fishes. Springer, Singapore. DOI：10.1007/978-981-97-1790-3_25.

Ganie PA, Posti R, Kunal K. 2023c. Modelling of the Himalayan Mountain river basin through hydro-morphological and compound factor-based approaches using geoinformatics tools. Modeling Earth Systems and Environment, 9(3): 3053−3084. DOI：10.1007/s40808-023-01691-9.

Ganie PA, Posti R, Kunal K, et al. 2022. Insights into the morphometric characteristics of the Himalayan River using remote sensing and GIS techniques: A case study of Saryu Basin, Uttarakhand, India. Applied Geomatics, 14(4): 707−730. DOI：10.1007/s12518-022-00461-z.

Gayen S, Bhunia GS, Shit PK. 2013. Morphometric analysis of Kangshabati-Darkeswar Interfuves area in West Bengal, India using ASTER DEM and GIS techniques. Journal of Geological Sciences, 2(4): 1−10. DOI：10.4172/2329-6755.1000133.

Geological Survey of India (GSI). 1981. Mineralogical map of Karnataka and Goa. Geological Survey of India.

Giusti EV, Schneider WJ. 1965. The distribution of branches in river networks. USGS professional paper, 422G, US Geological Survey. DOI：10.3133/pp422G.

Gottschalk LC. 1964. Reservoir sedimentation reservoir sedimentation. In: Chow VT, Ed. , Handbook of Applied Hydrology, McGraw Hill Book Company, New York.

Guth PL. 2011. Drainage basin morphometry: A global snapshot from the shuttle radar topography mission. Hydrology and Earth System Sciences, Copernicus Publications. European Geosciences Union. DOI：10.5194/hess-15-

2091-2011.

Gustafson GU, Krásný J. 1994. Crystalline rock aquifers: Their occurrence, use and importance. Applied Hydrogeology, 2: 64−75. DOI: 10.1007/s100400050051.

Lü QT, Yan JY, Chen XH, et al. 2020. Progress of deep geological survey project under the China geological survey. China Geology, 3(1): 153−72. DOI: 10.31035/cg2020001.

Hoek E, Marinos P, Marinos V. 2005. Characterization and engineering properties of tectonically undisturbed but lithologically varied sedimentary rock masses. International Journal of Rock Mechanics and Mining Sciences, 42/2: 277−285. DOI: 10.1016/j.ijrmms.2004.09.015.

Horton RE. 1932. Drainage-basin characteristics. Transactions, American Geophysical Union, 13(1): 350−361. DOI: 10.1029/TR013i001p00350.

Horton RE. 1945. Erosional development of streams and their drainage basins, hydrophysical approach to quantitative morphology. Geological Society of America Bulletin, 56(3): 275−370. DOI: 10.1130/0016-7606(1945)56[275:EDOSAT]2.0.CO;2.

Howard AD. 1990. Theoretical model of optimal drainage networks. Water Resources Research, 26(9): 2107−2117. DOI: 10.1029/WR026i009p02107.

Joshi LM, Kotlia BS. 2015. Neotectonically triggered instability around the palaeolake regime in Central Kumaun Himalaya, India. Quaternary International, 371: 219−231. DOI: 10.1016/j.quaint.2014.10.033.

Kabite G, Gessesse B. 2018. Hydro-geomorphological characterization of Dhidhessa River Basin, Ethiopia. International Soil and Water Conservation Research, 6: 175−83. DOI: 10.1016/j.iswcr.2018.02.003.

Kaplan D, Hegarty CJ. 2006. Understanding GPS: Principles and applications. Artech House, Boston, London, 32.

Kačaroğlu F. 1999. Review of groundwater pollution and protection in karst areas. Water, Air, and Soil Pollution, 113: 337−356. DOI: 10.1023/A:1005014532330.

Khatoon T, Javed A. 2022. Morphometric behavior of Shahzad Watershed, Lalitpur District, Uttar Pradesh, India: A geospatial approach. Journal of Geographic Information System, 14(3): 193−220. DOI: 10.4236/jgis.2022.143011.

Krishnan A, Ramasamy J. 2022. Morphometric assessment and prioritization of the South India Moyar river basin sub-watersheds using a geo-computational approach. Geology, Ecology, and Landscapes, 1−11. DOI: 10.1080/24749508.2022.2109819.

Kumar L, Joshi G, Agarwal KK. 2020. Morphometry and morphostructural studies of the parts of Gola River and Kalsa River Basins, Chanphi-Okhalkanda Region, Kumaun Lesser Himalaya, India. Geotectonics, 54(3): 410−427. DOI: 10.1134/S0016852120030048.

Kumar N, Singh SK, Singh VG, et al. 2018. Investigation of impacts of land use/land cover change on water availability of Tons River Basin, Madhya Pradesh, India. Modeling Earth System Environment, 4: 295−310. DOI: 10.1007/s40808-018-0425-1.

Lachassagne P, Dewandel B, Wyns R. 2021. Hydrogeology of weathered crystalline/hard-rock aquifers—guidelines for the operational survey and management of their groundwater resources. Hydrogeology Journal, 29(8): 2561−94. DOI: 10.1007/s10040-021-02339-7.

Loritz R, Kleidon A, Jackisch C, et al. 2019. A topographic index explaining hydrological similarity by accounting for the joint controls of runoff formation. Hydrology and Earth System Sciences, 23(9): 3807−3821. DOI: 10.5194/hess-23-3807-2019.

Mahadevaswamy G, Nagaraju D, Siddalingamurthy S, et al. 2011. Morphometric analysis of Nanjangud taluk, Mysore District, Karnataka, India, using GIS Techniques. International Journal of Geomatics and Geosciences, 1(4): 721−734.

Miller VC. 1953. A quantitative geomorphologic study of drainage basin characteristics in the Clinch Mountain area, Virginia and Tennessee, Project NR 389-042, Tech Report 3. Columbia University.

Mohamed E. 2020. Watershed delineation and morphometric analysis using remote sensing and GIS mapping techniques in Qena-Safaga-Bir Queh, Central Eastern Desert. Interna-

tional Journal of Water Resources and Environmental Engineering, 12(2): 22–46. DOI：10.5897/ijwree2019.0896.

Moharir K, Pande C, Patode RS, et al. 2021. Prioritization of sub-watersheds based on morphometric parameter analysis using geospatial technology. Water Management and Water Governance: Hydrological Modeling, 19−33. DOI: 10.1007/978-3-030-58051-3_2

Morris DG, Heerdegen RG. 1988. Automatically derived catchment boundaries and channel networks and their hydrological applications. Geomorphology, 1(2): 131−141. DOI：10.1016/0169-555X(88)90011-6.

Mustak SK, Baghmar NK, Ratre CR. 2012. Measurement of dissection index of Pairi River basin using remote sensing and GIS. National Geographical Journal of India, 58(2): 97−106.

Muthamilselvan A, Rajasekaran N, Suresh R. 2019. Mapping of hard rock aquifer system and artificial recharge zonation through remote sensing and GIS approach in parts of Perambalur District of Tamil Nadu, India. Journal of Groundwater Science and Engineering. 7(3): 264−281. DOI：10.19637/j.cnki.2305-7068.2019.03.007.

Nag SK, Chakraborty S. 2003. Influence of rock types and structures in the development of drainage network in hard rock area. Journal of the Indian Society of Remote Sensing, 31(1): 25–35. DOI：10.1007/BF030 30749.

Nag SK. 1998. Morphometric analysis using remote sensing techniques in the Chaka subbasin, Purulia district, West Bengal. Journal of the Indian Society of Remote Sensing, 26(1): 69−76. DOI：10.1007/BF03007341.

Neuzil CE. 1994. How permeable are clays and shales? Water resources research, 30(2): 145−150. DOI：10.1029/93WR02930.

Nikhil Raj PP, Azeez PA. 2012. Morphometric analysis of a tropical medium river system: A case from Bharathapuzha river southern India. Open Journal of Modern Hydrology, 02: 91−98. DOI：10.4236/ojmh.2012.24011.

Olszevski N, Fernandes Filho EI, Costa LM, et al. 2011. Morphology and hydrological aspects of Black River Basin, division of state of Rio de Janeiro and Minas Gerais. Revi Árvore, 35(3): 485–492. DOI：10. 1590/S0100-67622011000300011.

Pankaj A, Kumar P. 2009. GIS-based morphometric analysis of fve major sub-watersheds of Song River, Dehradun District, Uttarakhand with special reference to landslide incidences. Journal of the Indian Society of Remote Sensing, 37(1): 157−166. DOI：10.1007/s12524-009-0007-9.

Phillips JD. 2006. Evolutionary geomorphology: Thresholds and nonlinearity in landform response to environmental change. Hydrology and Earth System Sciences, 10(5): 731−742. DOI：10.5194/hess-10-731-2006.

Rai PK, Mohan K, Mishra S, et al. 2017. A GIS-based approach in drainage morphometric analysis of Kanhar River Basin, India. Applied Water Science, 7(1): 217−232. DOI：10.1007/s13201-014-0238-y.

Reddy GP, Maji AK, Gajbhiye KS. 2004. Drainage morphometry and its infuence on landform characteristics in a basaltic terrain, Central India–a remote sensing and GIS approach. International Journal of Applied Earth Observation and Geoinformation, 6(1): 1–16. DOI：10.1016/j.jag.2004.06.003.

Saha S, Das J, Mandal T. 2022. Investigation of the watershed hydro-morphologic characteristics through the morphometric analysis: A study on Rayeng basin in Darjeeling Himalaya. Environmental Challenges, 7: 100463. DOI：10.1016/j.envc.2022.100463.

Schumm SA. 1956. Evolution of drainage systems and slopes in badlands at Perth Amboy, New Jersey. Geological Society of America Bulletin, 67(5): 597−646. DOI：10.1130/0016-7606(1956)67[597:EODSAS]2.0.CO;2.

Selvan MT, Ahmad S, Rashid SM. 2011. Analysis of the geomorphometric parameters in high altitude glaciered terrain using SRTM DEM data in Central Himalaya, India. ARPN Journal of Science and Technology, 1(1): 22−27.

Shekar PR, Mathew A. 2022. Evaluation of morphometric and hypsometric analysis of the Bagh River basin using remote sensing and geographic information system techniques. Energy Nexus, 7: 100−104. DOI：10.1016/j.nexus.2022.100104.

Shrestha AB, Bajracharya SR, Sharma AR, et al. 2017. Observed trends and changes in daily temperature and precipitation extremes over

the Koshi river basin 1975–2010. International Journal of Climatology, 37(2): 1066–1083. DOI：10.1002/joc.4761.

Singh S, Singh MB. 1997. Morphometric analysis of Kanhar river basin. National Geographical Journal of India, 43(1): 31−43.

Smith KG. 1950. Standards for grading texture of erosional topography. American Journal of Science, 248(9): 655−668. DOI：10.2475/ajs.248.9.655.

Sreedevi PD, Owais SHHK, Khan HH, et al. 2009. Morphometric analysis of a watershed of South India using SRTM data and GIS. Journal of Geological Society of India, 273(4): 543−552. DOI：10.1007/s12594-009-0038-4.

Strahler AN. 1952. Hypsometric (area-altitude) analysis of erosional topography. Geological Society of America Bulletin, 63(11): 1117−1142. DOI：10.1130/0016-7606(1952)63[1117:HAAOET]2.0.CO;2.

Strahler AN. 1957. Quantitative analysis of watershed geomorphology. Eos, Transactions American Geophysical Union, 38(6): 913−920. DOI：10.1029/TR038i006p00913.

Strahler AN. 1964. Part II. Quantitative geomorphology of drainage basins and channel networks. In: Chow V, Ed., Handbook of Applied Hydrology, McGraw Hill, New York, 439−476.

Subayani AM, Qari MH, Matsah MI. 2012. Digital elevation model and multivariate statistical analysis of morphometric parameters of some wadis, western Saudi Arabia. Arabian Journal of Geosciences, 5(1): 147−157. DOI：10.1007/s12517-010-0149-7.

Tarboton DG, Baker ME. 2008. Towards an algebra for terrain-based flow analysis. Representing, Modeling and Visualizing the Natural Environment: Innovations in GIS, 13: 167−194. DOI：10.1201/9781420055504.

Tassew BG, Belete MA, Miegel K. 2021. Assessment and analysis of morphometric characteristics of Lake Tana sub-basin, Upper Blue Nile Basin, Ethiopia. International Journal of River Basin Management, 21(2): 195−209. DOI：10.1080/15715124.2021.1938091.

Thomas J, Joseph S, Thrivikramaji KP. 2010. Morphometric aspects of a small tropical mountain river system, the southern Western Ghats, India. International Journal of Digital Earth, 3(2): 135−156. DOI：10.1080/17538940903464370.

UNAVCO facility. Geoid height calculator, Accessed on on 20 August 2024.

Valdiya KS. 1976. Himalayan transverse faults and folds and their parallelism with subsurface structures of North Indian plains. Tectonophysics, 32(3/4): 353−386. DOI：10.1016/0040-1951(76)90069-X.

Valdiya KS. 1980. Geology of Kumaun lesser Himalaya (Vol. 280). Wadia Institute of Himalayan Geology. Rajpur Road Dehradun: Himachal times press.

Vijith H, Satheesh R. 2006. GIS-based morphometric analysis of two major upland sub-watersheds of Meenachil river in Kerala. Journal of the Indian Society of Remote Sensing, 34(2): 181−185. DOI：10.1007/BF02991823.

Vinutha DN, Janardhana MR. 2014. Morphometry of The Payaswini Watershed, Coorg District, Karnataka, India, using remote sensing and GIS techniques. International Journal of Innovative Research in Science, Engineering and Technology, 3(5): 516–24.

Vyas S, Singh GP. 2020. Morphometric analysis of hard rock terrain of Banne watershed, District Chattarpur, Madhya Pradesh, India using remote sensing and GIS. International Journal on Emerging Technologies, 11(2): 714−721.

Wilson JSJ, Chandrasekar N, Magesh NS. 2012. Morphometric analysis of major sub-watersheds in Aiyar & Karai Pottanar Basin, Central Tamil Nadu, India using remote sensing & GIS techniques. Bonfring International Journal of Industrial Engineering and Management Science, 2 (Special Issue on Geospatial Technology Development in Natural Resource and Disaster Management), 08-15.

Zhai X, Zhang Y, Zhang Y, et al. 2021. Simulating flash flood hydrographs and behavior metrics across China: Implications for flash flood management. Science of the Total Environment, 763: 142977. DOI：10.1016/j.scitotenv.2020.142977.